NASA CR-54986
GA-7190

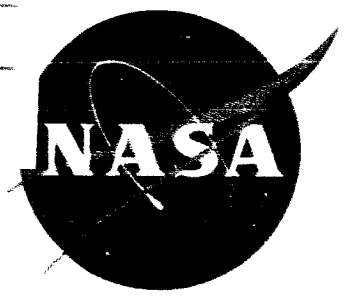

TUNGSTEN NUCLEAR ROCKET

PHASE II

FINAL REPORT

Part 1

prepared for

NATIONAL AERONAUTICS AND SPACE ADMINISTRATION

Contract SNPC-27

by

GENERAL ATOMIC

DIVISION OF

GENERAL DYNAMICS

JOHN JAY HOPKINS LABORATORY FOR PURE AND APPLIED SCIENCE

P.O. BOX 608 SAN DIEGO 12, CALIFORNIA

NOTICE

This report was prepared as an account of Government-sponsored work. Neither the United States, nor the National Aeronautics and Space Administration (NASA), nor any person acting on behalf of NASA:

A.) Makes any warranty or representation, expressed or implied, with respect to the accuracy, completeness, or usefulness of the information contained in this report, or that the use of any information, apparatus, method, or process disclosed in this report may not infringe privately owned rights; or

B.) Assumes any liabilities with respect to the use of, or for damages resulting from the use of, any information, apparatus, method or process disclosed in this report.

As used above, "person acting on behalf of NASA" includes any employee or contractor of NASA, or employee of such contractor, to the extent that such employee or contractor of NASA, or employee of such contractor, prepares, disseminates, or provides access to, any information pursuant to his employment or contract with NASA, or his employment with such contractor.

Requests for copies of this report should be referred to

National Aeronautics and Space Administration
Office of Scientific and Technical Information
Attention: AFSS-A
Washington, D.C. 20546

GENERAL ATOMIC

DIVISION OF

GENERAL DYNAMICS

JOHN JAY HOPKINS LABORATORY FOR PURE AND APPLIED SCIENCE

P.O. BOX 608, SAN DIEGO, CALIFORNIA 92112

NASA CR-54986
GA-7190

TUNGSTEN NUCLEAR ROCKET
PHASE II
FINAL REPORT

Part 1

June 15, 1966

Work done by:

R. G. Bardes
C. F. Bohren
S. C. Cohen
E. M. Gillette
G. F. Hoover
G. D. Joanou
L. O. Lavigne
J. M. Lovallo
J. C. Peak
N. Smith
L. Stewart

Report written by:

R. G. Bardes
C. F. Bohren
S. C. Cohen
J. C. Peak

prepared for

NATIONAL AERONAUTICS AND SPACE ADMINISTRATION

Contract SNPC-27

Technical Management
NASA-Lewis Research Center
Cleveland, Ohio
Nuclear Systems Division
D. Bogart

CONTENTS

LIST OF ILLUSTRATIONS

I. INTRODUCTION

This final report describes the critical experiments and nuclear analysis performed under Phase II of Contract SNPC-27 during the period January 16, 1966, through June 15, 1966. This work was part of a feasibility study of the Tungsten Water-Moderated Nuclear Rocket Reactor being conducted by NASA-Lewis Research Center. The reactor concept utilizes tungsten metal enriched in the low capture cross section isotope W^{184} to attain high temperature performance capabilities with a reasonable fissile material inventory.

During Phase I of the contract, the critical facility was put into operation and critical experiments were performed using unzoned cores. Analytical methods were reviewed and the critical experiments were analyzed. Neutron capture cross sections were measured for the tungsten isotopes, and cross section data for other isotopes were evaluated. A final report on Phase I has been published.[1]

During Phase II, which completes Contract SNPC-27, critical experiments were performed on two zoned cores. The experiments were analyzed using the methods developed in Phase I.

This report is published in two parts, each under separate cover, to facilitate distribution of the unclassified portion, which is contained in this part. It has been organized as follows: Section II contains a brief description of the critical facility and the zoned critical assemblies; Section III describes the experimental methods and results; Section IV describes the analytical methods and compares the results to the experiments; Section V gives a discussion of the results and the conclusions. Three appendices on various aspects of the analytical methods are also provided.

The final report of Phase I (NASA CR-54909) listed the reports and papers issued during 1964 and 1965. The following list contains reports and papers published during 1966 aside from this final report:

1. "Supplemental Hazards Analysis for the General Atomic Tungsten Nuclear Rocket Critical Facility, "by Tungsten Nuclear Rocket Staff, in a letter from D. W. Ver Planck, Acting Director of the Laboratory of the General Atomic Division, to Roger S. Boyd, Chief, Research and Power Reactor Safety Branch, Division of Reactor Licensing, USAEC, January 28, 1966.

2. R. G. Bardes, et al., "Tungsten Nuclear Rocket Phase I, Final Report. "NASA Report NASA CR-54909, General Atomic Division, General Dynamics Corporation, April 22, 1966.

3. S. C. Cohen, "An Improved Treatment of Scattering Resonances in Slab Geometry, "General Atomic Report GA-7144, May 13, 1966, submitted for publication as a technical note in Nuclear Science and Energy".

4. R. G. Bardes, C. F. Bohren, S. C. Cohen, E. M. Gillette, J. M. Lovallo, R. A. Moore, and J. C. Peak, "Experimental and Analytical Results on the Tungsten Water-Moderated Nuclear Rocket Critical Assembly, " Trans. Am. Nuc. Soc. 9, 1, (1966).

5. S. C. Cohen, R. G. Bardes, and J. C. Peak, "Isothermal Temperature Coefficient of the Tungsten Water-Moderated Rocket Critical Assembly, "Trans. Am. Nuc. Soc. 9, 1, (1966).

6. S. C. Cohen, and C. A. Stevens, "Resonance Calculations for Multiple Body Annular Rings With an Interstitial Scatterer, "Trans. Am. Nuc. Soc. 9, 1, (1966).

II. NUCLEAR ROCKET CRITICAL FACILITY

2.1 DESCRIPTION OF CRITICAL FACILITY

The Critical Assembly consists of a reactor, water dump tank, associated plumbing, safety and regulating rods, control and research instrumentation, and control circuitry.

Figure 2.1 shows design details of the reactor tank assembly. The basic structural element of the critical assembly is the reactor tank base plate, which is a 1-1/4-in. thick aluminum plate seven feet in diameter mounted on four braced support legs.

The cylindrical reactor shroud is bolted to the base plate to form a reactor tank 78 in. in diameter and 82 in. deep. The aluminum core support plate, which is 3/4 in. thick and five feet in diameter is mounted on six standoffs on the base plate.

Fuel element and poison tube positioning is accomplished by using two aluminum grid plates. Figure 2.2 shows the general grid plate layout and the identification system; upper case letters refer to fuel element positions and lower case letters to poison tube positions. There are 127 fuel element positions and 216 poison tube positions.

The core thus consists of an array of fuel elements and poison tubes held vertically at the proper spacing by the grid plates, with all removable elements resting on the core support plates. A more detailed description of the critical facility is given in Section 2.2 of Ref. 1.

The core excess reactivity was adjusted by neutron absorption in a cadmium nitrate solution contained in nickel-plated aluminum tubes.

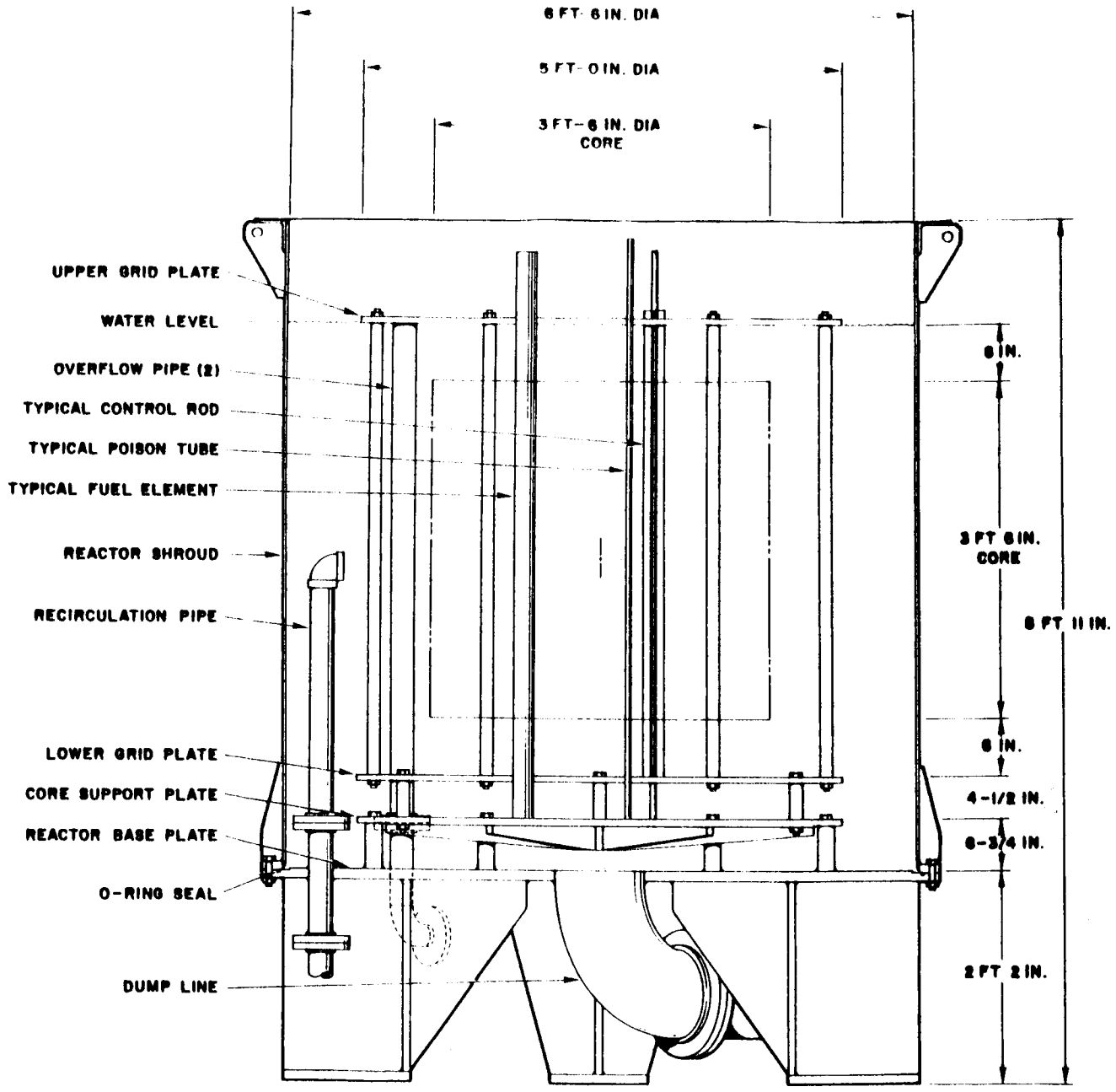

Fig. 2.1--Reactor tank assembly

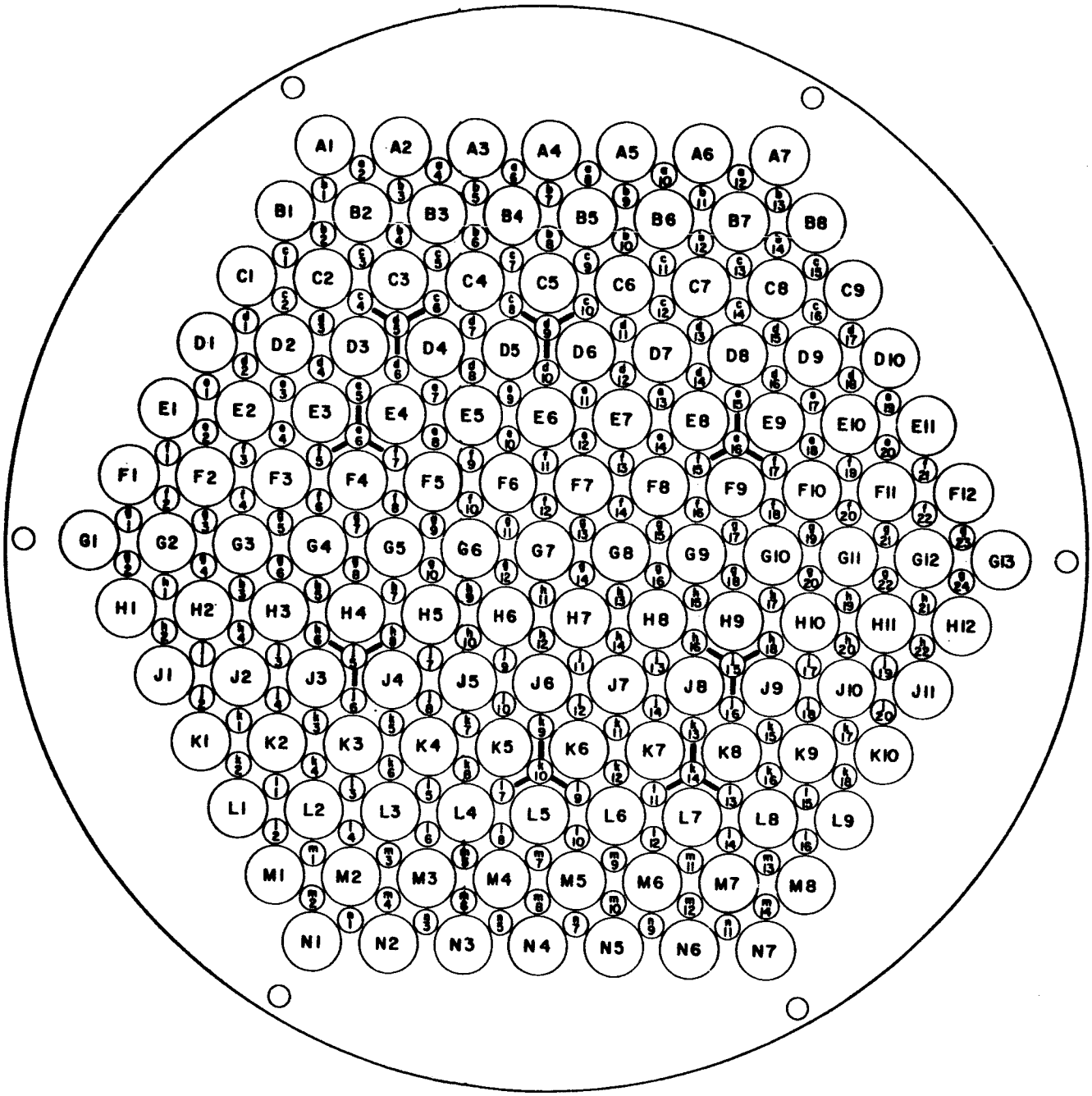

Fig. 2.2--Grid plate identification scheme

The tubes were sealed at the ends with a double seal. One seal was a standard O-ring and the other a tight mechanical seal formed by magnetically swaging the tube over the end plug.

Various concentrations of cadmium nitrate were used during the experimental program. Table 2.1 is a summary of the concentrations used.

Table 2.1

POISON CONCENTRATIONS AND COLOR CODE

Type	Color Code	Concentration (Moles/liter)	Remarks
K	Copper	0.2202	Core III Final Concentration
M	Light Green	0.1704	Core IV Final Concentration
N	Light Blue	0.1278	Core V Final Concentration

The fuel element assembly and subassembly are shown in Fig. 2.3. The subassembly consists of 24 stages each containing five concentric rings of uranium-aluminum alloy and one ring of depleted uranium. These rings are lined with natural tungsten and are positioned on thin-wall aluminum tubing. The fuel rings contain approximately 35 wt % metallic uranium, which is 93.15% enriched. The rings are 0.042 in. thick and 1-5/8 in. high. The stages are separated axially by 1/8-in. corrugated aluminum spacer rings. These spacer rings also position the fuel radially in the element.

Each fuel ring is lined on the inside with 0.005 in. of natural tungsten. The outermost ring of the subassembly is 0.040-in. thick depleted uranium and is lined on the inside with an 0.003-in. ring of natural tungsten. Additional tungsten was also added for zoning purposes; the additions are described in Section 2.2.

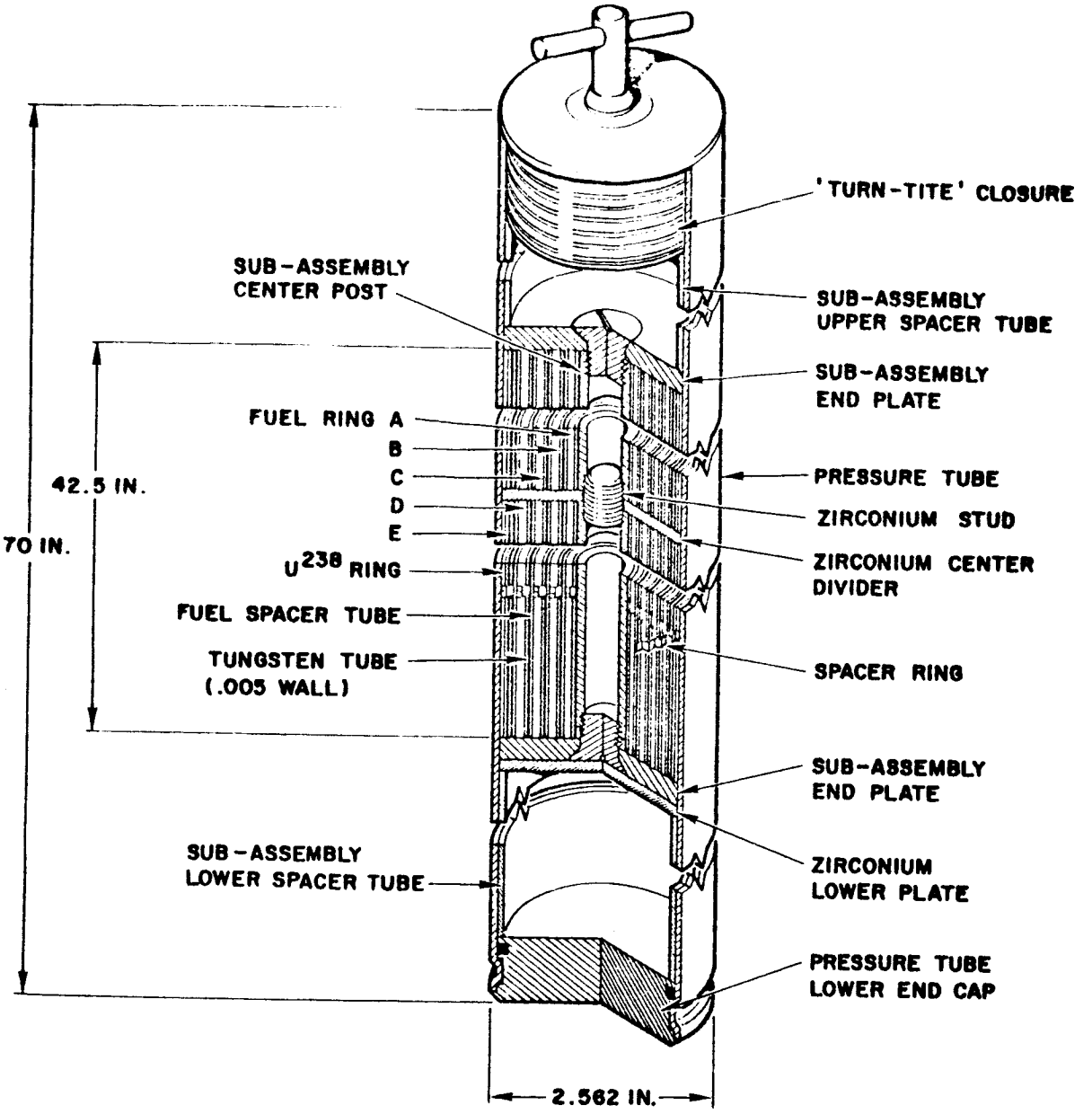

Fig. 2.3--Fuel element

The pressure tubes were made from 6061-T3 aluminum and have an average o.d. of 2.562 in. and a wall thickness of 0.065 in.

2.2 COMPARISON OF CORE CONFIGURATIONS

Two distinct core configurations were used throughout Phase II of the experimental program. They have been sequentially numbered in the order in which they were built. Both cores used the identical reactor structure, control rods, reflector configuration, and pitch as Core III of Phase I. They differed only in the amount of natural tungsten added for zoning.

2.2.1 CORE III

The third core built during Phase I used the original 3.00-in. pitch grid plates. However, the side and bottom reflectors were made primarily of beryllium metal and the top reflector was water (with voids) 2.0 in. thick. In addition, the subassembly axial spacers were removed from the fuel elements so that the subassemblies rested on the bottom of the pressure tubes.

Figures 2.4 and 2.5 show the mounting of the side beryllium reflectors. The scalloped aluminum faceplates on the beryllium boxes were designed so that the amount of water around the edge cells would be the same as that around the interior core cells. The polyethylene shown in Fig. 2.5 was used to give a better simulation of the reference design which has cooling water in the reflector. The boral sheet approximated a thermal neutron vacuum boundary, which exists in the reference design. Grid plate locations A-1, A-7, G-13, N-7, N-1, and G-1 were filled with voided pressure tubes.

The bottom beryllium reflector, which is shown in Fig. 2.6, is contained in a leakproof aluminum container that fits between the core support plate and the bottom grid plate. When the bottom reflector is in position, the fuel elements are supported by the reflector container.

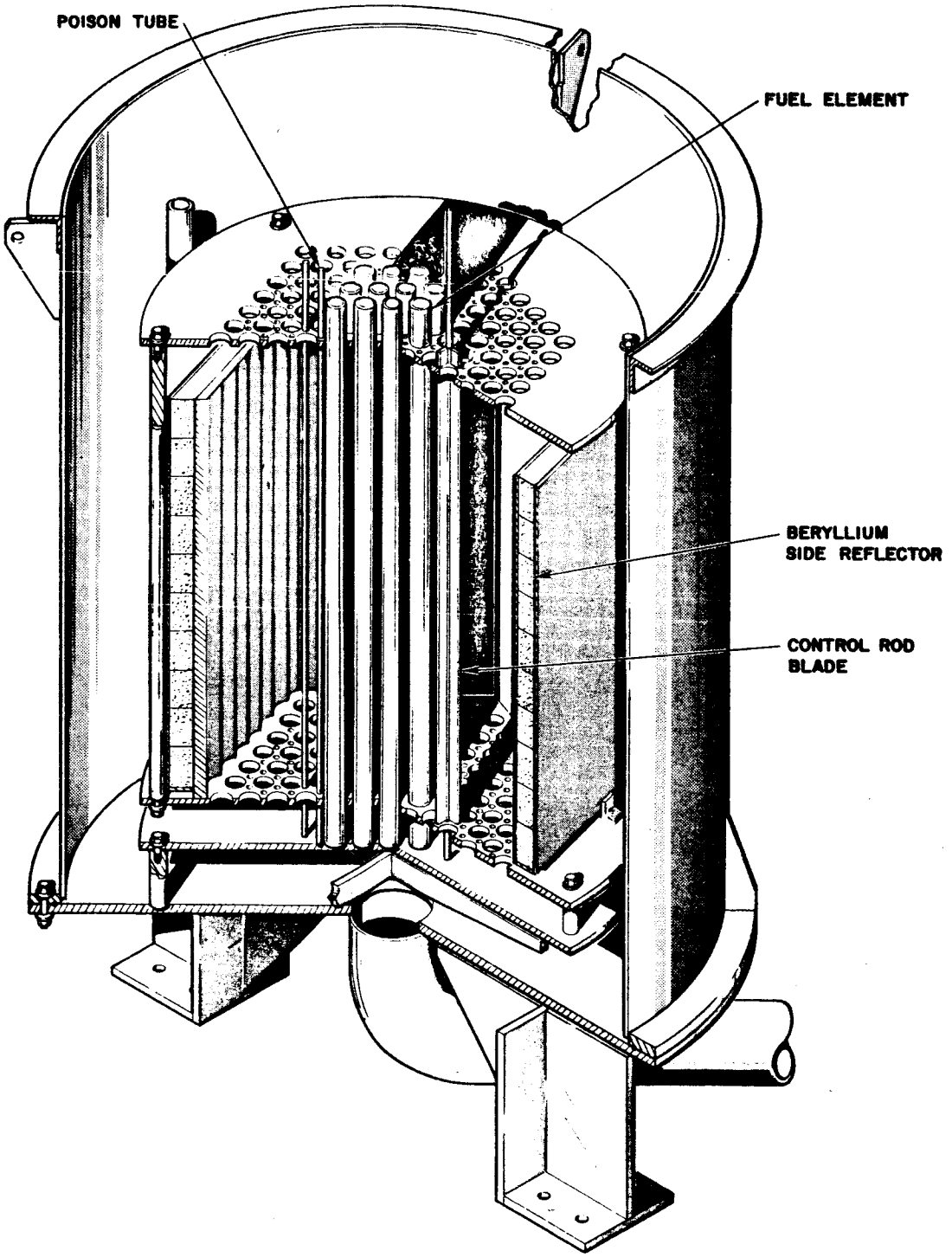

Fig. 2.4--Cross section of reactor tank and core support structure

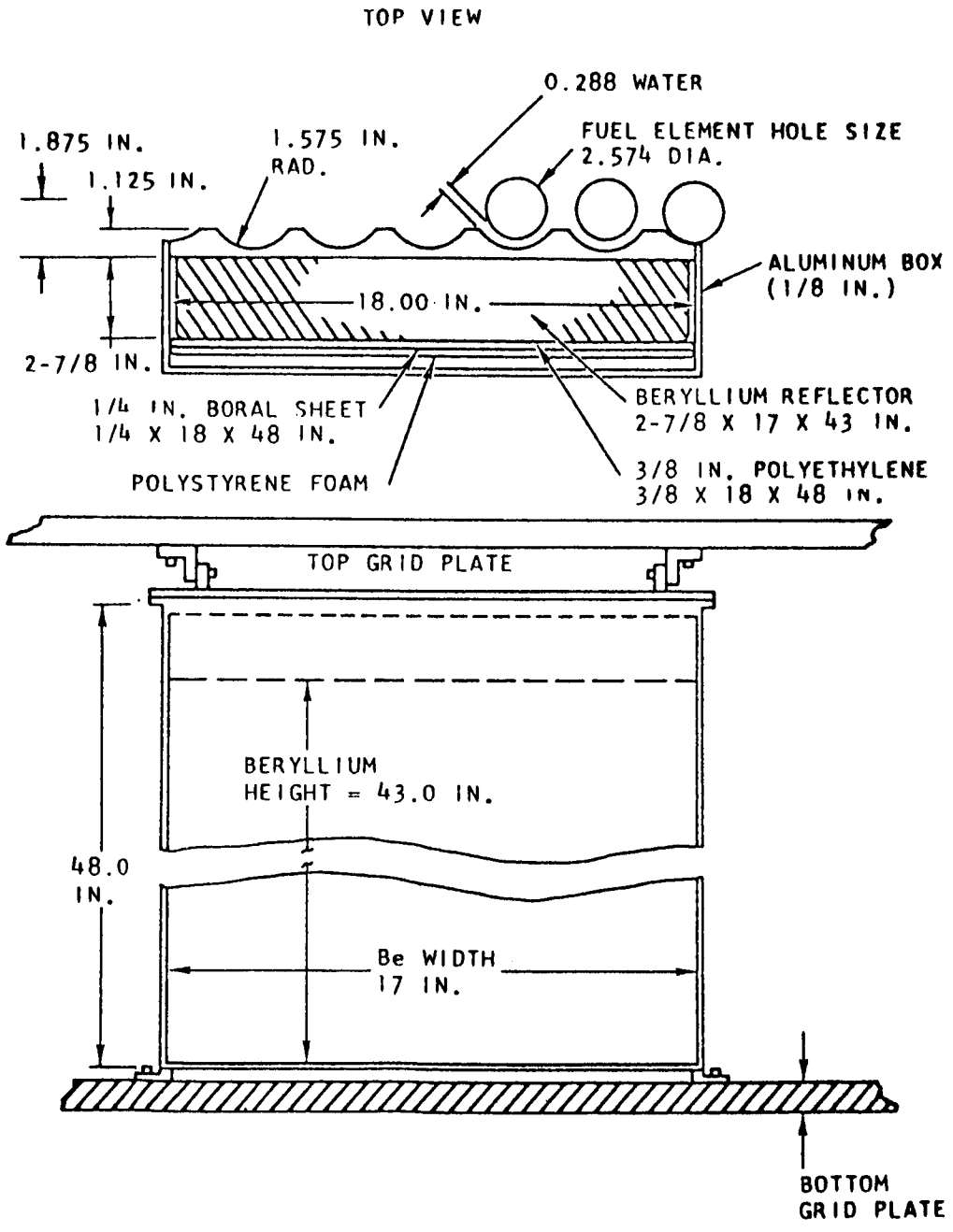

Fig. 2.5--Side reflector, 3.0-in. pitch, Be-reflected core

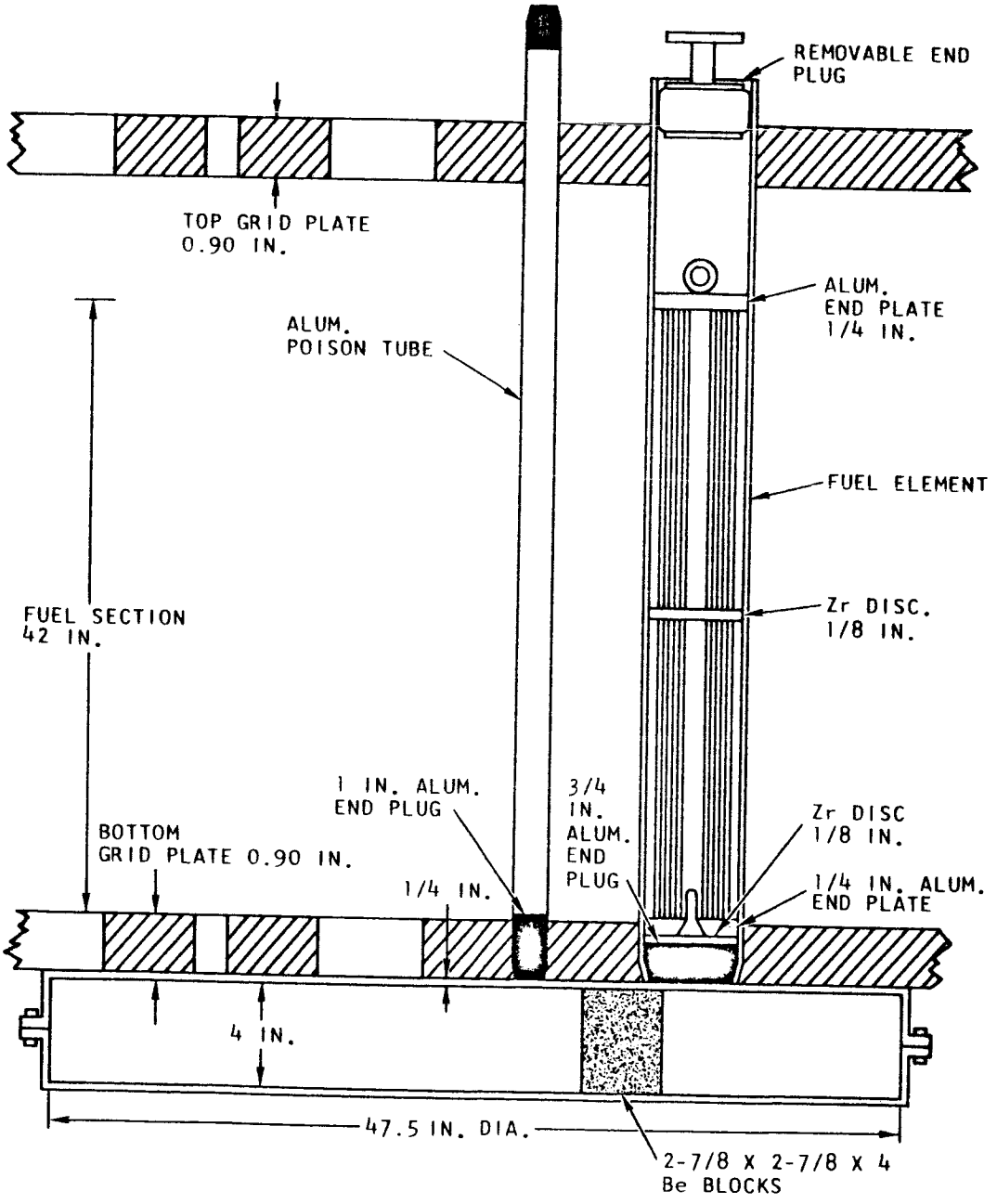

Fig. 2.6--Bottom reflector, 3.0-in. pitch, Be-reflected core

2.2.2 CORE IV

Core IV, constructed under Phase II, is identical to Core III except for the central 19 fuel elements. Each of the latter contains an additional 10-mil tungsten ring located on the outside of the U^{238} ring. Table 2.2 shows the weight distribution of the added 10-mil tungsten rings.

Table 2.2

WEIGHT DISTRIBUTION OF 10-MIL TUNGSTEN RINGS

Weight (gm)	Quantity
32.0 - 32.9	11
33.0 - 33.9	35
34.0 - 34.9	65
35.0 - 35.9	110
36.0 - 36.9	94
37.0 - 37.9	75
38.0 - 38.9	53
39.0 - 39.9	32
40.0 -	17

2.2.3 CORE V

Core V was constructed from Core IV by adding a 50-mil tungsten ring to Stages 11 through 19 of every fuel element. The 50-mil tungsten rings were located on the outside of fuel ring "A" and had the weight distribution shown in Table 2.3.

Table 2.3

WEIGHT DISTRIBUTION OF 50-MIL TUNGSTEN RINGS

Weight (gm)	Quantity
70.0 - 70.9	16
71.0 - 71.9	74
72.0 - 72.9	293
73.0 - 73.9	360
74.0 - 74.9	248
75.0 - 75.9	111

III. EXPERIMENTAL METHODS AND RESULTS

3.1 CORE LOADING

Core IV was constructed by adding 10-mil tungsten rings to the 19 central fuel elements of Core III. This resulted in a subcritical configuration. The cadmium concentration in the poison tubes was then reduced to compensate for the added tungsten. The inverse source multiplication technique was used to limit the number of lower concentration poison tubes inserted in a single loading step. The same procedure was followed in constructing Core V from Core IV.

A "standard core" has been defined for comparison of results. This core contains 121 fuel elements, 204 poison tubes, no rod guides, and no source tube. Poison locations a-2, b-1, a-12, b-13, g-23, g-24, m-14, n-11, n-1, m-2, g-2 and g-1 (used to shim the core to the desired excess reactivity) were defined to contain water-filled tubes in the standard core. Locations d-9, e-16, j-15, k-10, d-5, k-15, j-5, and e-6, which contain the control rod guides, and location h-10, which contains the source tube, were defined to be filled with poison tubes in the standard core. Experimental corrections were made in the following results to account for the missing poison tubes at these locations. This was done by measuring the reactivity difference between a stainless steel rod guide or source tube and a poison tube at equivalent locations. Experimental corrections were also made to account for the shim poison tubes and for fuel elements if less than 121 elements were loaded.

Table 3.1 shows the corrected excess reactivities for the two standard cores that were investigated in Phase II.

Table 3.1

EXCESS REACTIVITY OF THE STANDARD CORES

Core	Poison Tube Type	Excess Reactivity ($)
IV (3.0-in. Pitch Beryllium-Reflected Radial Zoning)	"M"	1.251
V (3.0-in. Pitch Beryllium-Reflected Radial and Axial Zoning)	"N"	0.136

3.2 REACTIVITY MEASUREMENTS

3.2.1 REGULATING AND SAFETY ROD WORTH

The regulating rods were calibrated by the period measurement technique. The total integrated single rod worth for Core IV was $0.496; for Core V it was $0.475. The safety rods were calibrated by the source multiplication technique; the inverse multiplication curve was generated by using the previously calibrated regulating rod to determine the amount by which the core was subcritical. The total integrated single rod worth was $0.56 each for Core IV and $0.56 each for Core V. The period measurement and source multiplication techniques are discussed in Section 3.2 of Ref. 1.

3.2.2 MEASUREMENT OF THE EXCESS REACTIVITY HELD DOWN BY CADMIUM SOLUTIONS

The grid plate contains 216 locations for poison tubes, rod guides, and the source. A total of 207 locations are available for cadmium poison tubes, nine locations being used by the eight stainless steel rod guides and the stainless steel source tube.

These 216 locations can be grouped into symmetric groups containing either six, twelve, or eighteen poison tubes at twenty distinct radii from the center of the core. Thus, it is possible to measure the

worth of representative groups of poison tubes, weight them by their occurrence, and add the results. This procedure is referred to as the reactivity mapping technique.

Table 3.2 shows the groupings and occurrence of a typical pattern. The poison tubes in each group were replaced with similar tubes containing pure water. The resultant reactivity change was then measured on the calibrated regulating rods.

Table 3.2

TYPICAL PATTERN USED IN DETERMINING THE TOTAL EXCESS REACTIVITY

Group	Poison Tubes	Weight Factor
1	f-11, f-7, j-18, k-1, h-11	6
2	c-14, e-8, g-15, k-5, l-16	12
3	j-14, k-6, c-3, f-2, g-23	12
4	j-16, e-18, d-3, j-1, a-8	12

A similar procedure was followed for mapping the worth of poison tubes having a higher cadmium concentration than the standard loading for a given core.

Table 3.3 shows the results obtained by mapping the worth of the standard poison tubes for each of the two primary cores. These results indicate what the total excess reactivity of a standard core would be if the cadmium nitrate solution in the poison tubes was replaced with pure water.

Table 3.3

EXCESS REACTIVITY OF STANDARD CORES WITHOUT CADMIUM IN POISON TUBES

Core	Excess Reactivity ($)
IV	18.432
V	14.242

3.2.3 POISON TUBE WORTH AT DIFFERENT RADIAL LOCATIONS

The reactivity change associated with the replacement of a tube filled with cadmium nitrate by a similar tube containing water was measured at various locations in Cores IV and V. The change in position of the calibrated regulating rods was used to determine the worth of the poison tubes. Table 3.4 presents the results obtained and Fig. 3.1 shows the results graphically.

Table 3.4

CADMIUM WORTH VS RADIUS

Location	Radius	Worth of Type "M" in Core IV ($)	Worth of Type "N" in Core V ($)
f-12	4.40	0.124	0.099
e-12	11.64	0.118	0.092
d-12	19.18	0.108	0.085
c-12	26.76	0.089	0.072
b-12	34.36	0.065	0.052
b-11	38.35	0.053	0.043

3.2.4 WORTH OF POISON TUBES HAVING DIFFERENT CADMIUM CONCENTRATIONS

The worth of the cadmium nitrate in a single poison tube as a function of the concentration was measured in Core V at location f-12.

The results are shown in Table 3.5 and in Fig. 3.2.

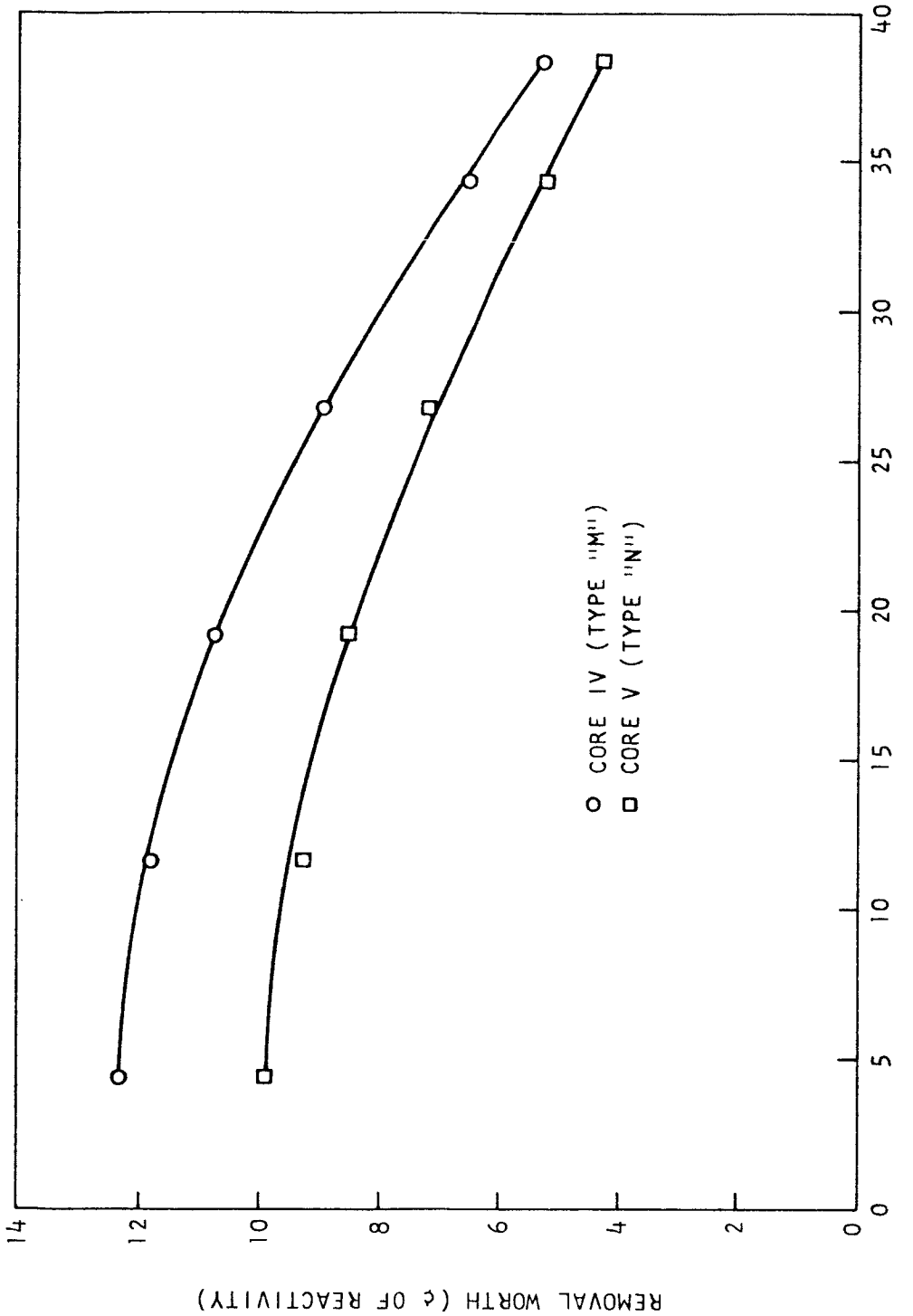

Fig. 3.1--Cadmium worth vs radius

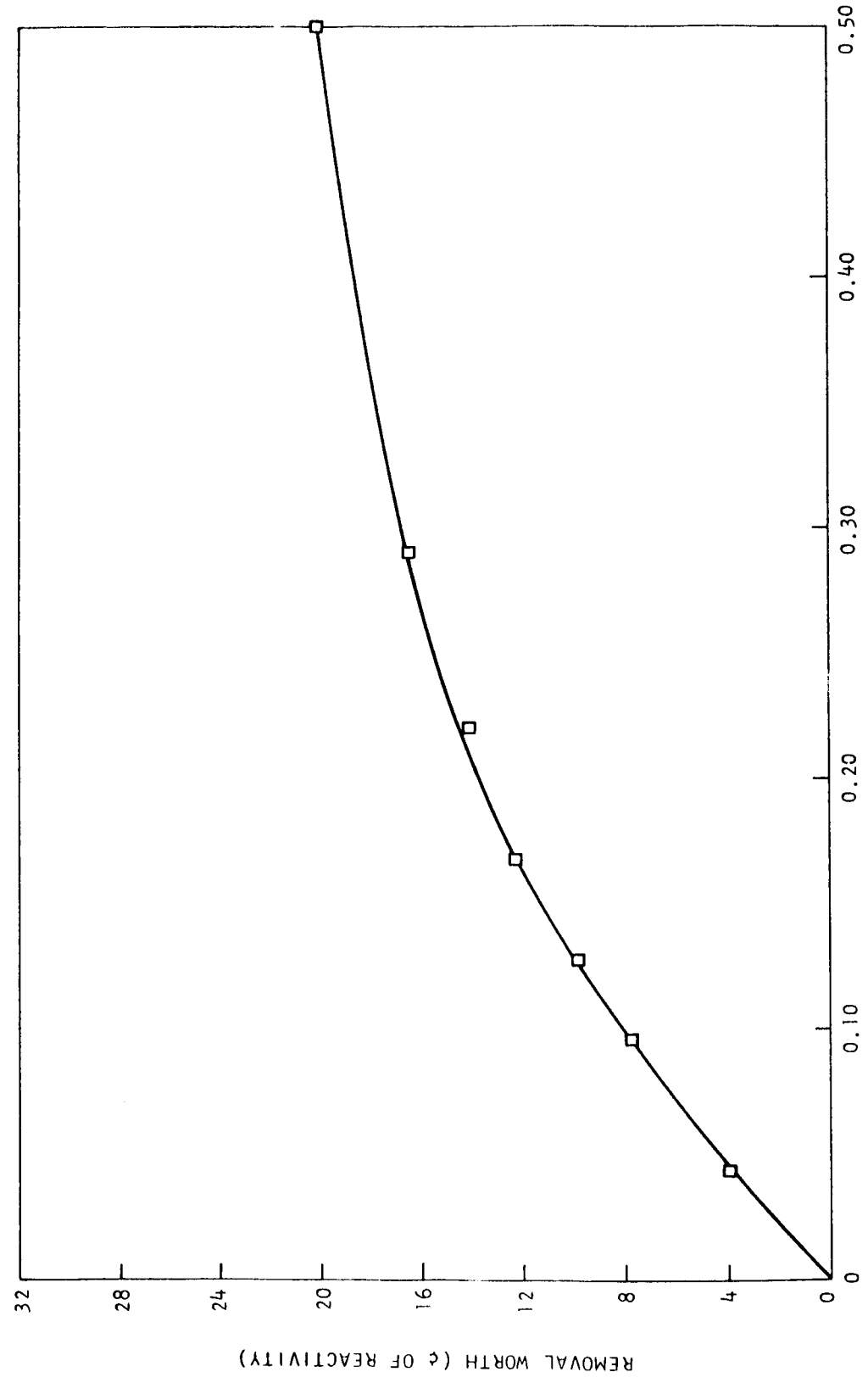

Fig. 3.2--Poison tube worth vs concentration - Core V

Table 3.5

POISON TUBE WORTH VS CADMIUM CONCENTRATION
(CORE V)

Cadmium Concentration (moles/liter)	Worth ($)
0.0431	0.039
0.06275	0.074
0.0956	0.106
0.1108	0.121
0.1255	0.132
0.1677	0.161
0.2202	---
0.250	0.201
0.290	---
0.500	0.275

3.2.5 WORTH OF TUNGSTEN ADDED FOR ZONING

The worth of the additional 10-mil tungsten rings used to zone Core IV was determined in the following way. The 10-mil tungsten rings were successively removed from the fuel elements in locations G-7, H-7, E-6, and G-5, and the increase in reactivity was measured for each of these four situations. The latter three locations have sixfold symmetry; thus, by multiplying each of these results by six and adding it to the value obtained in G-7, the reactivity worth of the additional tungsten in the central 19 elements could be determined. A removal worth of $2.36 was found for the added 10-mil tungsten by this method.

To determine the worth of the 50-mil tungsten rings used for axial zoning in Core V, the rings were removed from selected fuel elements and the reactivity change measured. By applying a symmetry factor to each of these changes, the total worth was determined as shown in Table 3.6.

Table 3.6

MAPPED WORTH OF 50-MIL TUNGSTEN RINGS

Fuel Element		Worth of Change ($)	Symmetry Factor	Worth of Group ($)
G-7		0.0412	1	0.041
G-6	E-3	0.0694	6	0.416
G-5	G-2	0.0452	6	0.271
G-10	K-1	0.0461	6	0.277
F-4	H-1	0.0406	12	0.487
J-1	F-11	0.0279	12	0.335
F-10	E-2	0.0578	12	0.694
F-5	G-3	0.0682	6	0.409
		Total removal worth of 50-mil tungsten rings		2.930

3.2.6 WORTH OF TUNGSTEN AND U^{238} RINGS IN CORE IV

To obtain an estimate of the total amount of reactivity held down by the tungsten and the U^{238} rings in Core IV, an experiment was conducted in which fuel elements containing no tungsten or U^{238} rings were substituted for the standard fuel elements at symmetrically reproducible locations. The results are shown in Table 3.7.

Table 3.7

WORTH OF TUNGSTEN AND U^{238} RINGS IN CORE IV

Location	Worth ($)	Symmetry	Total Worth ($)
K-1	0.1699	6	1.019
J-1	0.1628	12	1.954
J-2	0.2109	12	2.531
J-3	0.2795	6	1.677
H-1	0.1312	12	1.574
H-2	0.1841	12	2.209
H-3	0.2599	12	3.119
H-4	0.3210	12	3.857
H-5	0.4945	6	2.962
G-2	0.1444	6	0.866
G-3	0.2257	6	1.354
G-4	0.3018	6	1.811
G-5	0.4736	6	2.842
G-6	0.5048	6	3.029
G-7	0.5197	1	0.520
	Total removal worth of tungsten and U^{238} rings		31.324

3.3 ACTIVATION MEASUREMENTS

3.3.1 METHOD

Power distributions were measured by counting the relative gamma activity of the fuel rings in an extensive region of the core. The gamma activity above 400 keV was counted for each fuel ring while it was being rotated about its axis. A small 120 rpm electric motor equipped with a series of aluminum mandrels was installed above a scintillation crystal for this purpose. By this means it was possible to average the variations in fuel density and also the azimuthal variation of fission product activity in fuel rings near the core-reflector interface.

3.3.2 RADIAL POWER DISTRIBUTION IN CORE IV

The radial power distribution at the Stage 12 level of Core IV was determined by gamma counting the E-rings for fission product activity in an area of the core that is symmetrically reproducible. Table 3.8 lists the results.

3.3.3 RADIAL AND AXIAL POWER DISTRIBUTION IN CORE V

The power distribution in Core V has been measured by counting the "E" uranium-aluminum fuel rings for gamma activity. The relative activities obtained in this way were corrected for decay by repetitive counting of the Stage 12 E-ring of fuel element G-7. The decay curve generated was then used to normalize all counts to the same counting time. Corrections were also made for the amount of U^{235} in each of the rings based on their weight.

Corrections to the E-ring data were also made to account for unit cell variation between zones. There are four different unit cells in Core V: (1) cells containing the normal amount of tungsten, (2) cells containing an additional 50-mil tungsten ring outside the "A" fuel ring,

(3) cells containing an additional 10-mil tungsten ring outside the U^{238} ring, (4) cells containing both the 10- and 50-mil tungsten rings. The calculated relative power in these cells is shown in Table 3.9.

Since these factors are normalized to 1.0 for the E-ring, an analytical correction to the experimental results was made by multiplying the relative experimental E-ring power by the appropriate column sum. The results, renormalized to the average core power are given in Table 3.10.

The renormalization was made so that the results of Table 3.10 represent the local stage power divided by the average stage power. The latter was obtained using the fuel element symmetry factors shown in Table 3.11.

3.4 TEMPERATURE COEFFICIENT MEASUREMENTS

3.4.1 METHOD

The change in reactivity associated with heating of the water in both cores was measured by the following procedure. First, since a predominantly negative temperature coefficient was anticipated, the core excess reactivity was adjusted to a value slightly in excess of $0.40. With the reactor at just delayed critical, the reactor tank water was circulated through the heater loop. The change in reactivity with increasing water temperature was compensated for by movement of the regulating rods. After reaching the desired higher temperature, the heater was put under proportional control and the system allowed to come to temperature equilibrium. The poison tube in position g-14 contained water with no cadmium and three iron-constantan thermocouples. Four thermocouples and one thermohm were positioned as shown in Table 3.12. There were also several iron-constantan thermocouples in the beryllium side reflector. Typically, a ten-degree centigrade increase in water temperature

Table 3.8

RADIAL POWER, STAGE 12

Fuel Element	No. of Similar Elements	% of Total Core Power in Group	% of Total Core Power in Fuel Element	Radius (cm)
K-1	6	4.8780	0.813	39.6
J-1	12	9.4080	0.784	40.3
J-2	12	9.0240	0.752	33.2
J-3	6	5.0880	0.848	26.4
H-1	12	9.7920	0.816	42.4
H-2	12	8.4240	0.702	34.9
H-3	12	10.1760	0.848	27.5
H-4	12	11.0640	0.922	20.2
H-5	6	5.5440	0.924	13.2
G-2	6	4.4820	0.747	38.1
G-3	6	4.7700	0.795	30.5
G-4	6	5.2260	0.871	22.9
G-5	6	5.4600	0.910	15.2
G-6	6	5.7000	0.950	7.62
G-7	1	0.9450	0.945	0.0

Table 3.9

RELATIVE POWER PER RING (CALCULATED)

	Cell Type			
	(1)	(2)	(3)	(4)
Ring A	.21926	.22559	.18696	.19271
B	.31732	.32581	.30208	.31023
C	.45323	.46353	.44454	.45462
D	.65507	.66514	.65074	.66070
E	1.0	1.0	1.0	1.0
SUM	2.64488	2.68007	2.58432	2.61826

Table 3.10

LOCAL-TO-AVERAGE CORE POWER PER STAGE IN CORE V

	Fuel Element and Radius														
	G-7	G-6	H-5	G-5	H-4	G-4	J-3	H-3	G-3	J-2	H-2	G-12	K-1	J-1	H-1
Stage	0.0	7.62	13.2	15.2	20.2	22.7	26.4	27.5	30.5	33.2	34.9	38.1	39.6	40.3	42.4
1	1.58	1.57	1.53	1.50	1.51	1.38	1.38	1.33	1.35	1.18	1.15	1.12	1.26	1.23	1.22
2	1.38	1.36	1.35	1.30	1.33	1.21	1.22	1.17	1.18	1.05	0.99	.98	1.12	1.08	1.12
3	1.40	1.34	1.38	1.34	1.36	1.28	1.21	1.25	1.22	1.08	1.05	1.05	1.14	1.09	1.15
4	1.45	1.40	1.42	1.39	1.42	1.35	1.28	1.31	1.27	1.14	1.11	1.09	1.21	1.15	1.21
5	1.53	1.52	1.50	1.42	1.48	1.41	1.36	1.34	1.33	1.22	1.19	1.16	1.25	1.20	1.29
6	1.55	1.54	1.52	1.47	1.53	1.44	1.40	1.37	1.34	1.26	1.21	1.19	1.27	1.24	1.34
7	1.54	1.58	1.54	1.48	1.53	1.42	1.41	1.44	1.32	1.24	1.17	1.23	1.34	1.28	1.30
8	1.53	1.60	1.55	1.48	1.53	1.44	1.40	1.45	1.34	1.23	1.16	1.22	1.34	1.28	1.31
9	1.59	1.55	1.54	1.46	1.53	1.47	1.44	1.38	1.30	1.27	1.13	1.19	1.28	1.27	1.32
10	1.55	1.51	1.47	1.42	1.49	1.44	1.41	1.35	1.29	1.24	1.11	1.15	1.26	1.23	1.31
11	1.39	1.37	1.38	1.33	1.40	1.28	1.29	1.25	1.21	1.11	1.03	1.07	1.12	1.14	1.21
12	1.27	1.28	1.27	1.24	1.29	1.21	1.21	1.16	1.15	1.04	.97	1.02	1.10	1.07	1.21
13	1.27	1.22	1.25	1.18	1.27	1.16	1.15	1.13	1.06	1.02	.95	.95	1.03	1.00	1.06
14	1.18	1.15	1.17	1.10	1.21	1.10	1.09	1.07	1.00	.98	.89	.90	.98	.93	.98
15	1.12	1.10	1.11	1.05	1.12	1.03	1.06	.97	.92	.89	.83	.87	.92	.89	.91
16	1.02	1.03	1.03	.98	1.04	.95	.99	.91	.87	.82	.77	.81	.85	.83	.85
17	.94	.90	.95	.90	.92	.88	.87	.87	.81	.78	.72	.72	.80	.75	.78
18	.86	.82	.87	.86	.84	.82	.81	.80	.74	.71	.66	.66	.75	.69	.70
19	.79	.77	.78	.77	.76	.76	.74	.70	.66	.64	.61	.62	.66	.63	.65
20	.73	.71	.73	.72	.71	.71	.69	.65	.62	.59	.54	.57	.62	.58	.60
21	.64	.63	.62	.62	.64	.63	.60	.58	.55	.52	.48	.50	.53	.51	.53
22	.54	.52	.53	.51	.53	.53	.51	.48	.46	.44	.40	.42	.45	.43	.45
23	.43	.43	.42	.42	.44	.43	.40	.41	.34	.35	.33	.34	.36	.35	.36
24	.35	.36	.36	.34	.37	.37	.34	.33	.31	.29	.28	.28	.29	.29	.30

Table 3.11

FUEL ELEMENT SYMMETRY FACTORS

Fuel Element	Symmetry Factor
G-7	1
G-6	6
H-5	6
G-5	6
H-4	12
G-4	6
J-3	6
H-3	12
G-3	6
J-2	12
H-2	12
G-12	6
K-1	6
J-1	12
H-1	12
	121

Table 3.12

LOCATION OF TEMPERATURE MEASURING SENSORS

Thermocouple	Radial Position	Axial Position
1	g-14	Lower Reflector Interface
2	g-14	Center of Core
3	g-14	Upper Reflector Interface
4	10 in. beyond the reflector interface at midcore height.	
(thermohm)	10 in. beyond the reflector interface at midcore height.	

could be reached in about one hour with another half-hour being required to attain sufficient equilibrium to enable a reliable positive drift measurement to be made at a fixed regulating rod setting. The water temperature measurements were generally uniform to within $\pm 0.25^{\circ}C$ after slightly more than 1/2 hour. The thermohm bridge measurement of the absolute temperature is accurate to about $\pm 0.02^{\circ}C$.

In all cases, the calibration of the regulating rods was checked at the higher temperature and found to be essentially identical with the room temperature calibration.

3.4.2 RESULTS

Table 3.13 shows the isothermal temperature dependence of the reactivity obtained for Cores IV and V.

Table 3.13

REACTIVITY LOSS DUE TO TEMPERATURE FOR CORES IV AND V

Core IV		Core V	
Core Temp. ($^{\circ}C$)	Reactivity Loss ($)	Core Temp. ($^{\circ}C$)	Reactivity Loss ($)
20.9	0.0000	20.9	0.0000
25.4	0.0070	25.4	0.0034
30.1	0.0229	30.2	0.0163
		34.8	0.0429
40.2	0.0722	40.0	0.0728
50.0	0.1421	50.0	0.1418
59.6	0.2275	59.8	0.2298
69.8	0.3415	70.0	0.3478
		80.1	0.4858

3.5 PULSED NEUTRON MEASUREMENTS

Core V was pulsed to determine the prompt mean lifetime and to check for any modal effects that may have been overlooked during previous pulsed neutron source experiments. The pulse source was located outside the beryllium reflector region as shown in Fig. 3.3. Using a calibrated regulating rod, the core was made \$0.368 subcritical. The values of α, the prompt neutron decay constant, obtained with the detector probe at several different locations are shown in Table 3.14.

Using an average α of -267.3 sec^{-1}, as obtained from the three in-core measurements, the value of $\bar{\ell}/\beta_{eff}$ derived is 0.0051. Taking $\beta_{eff} = 0.00703$ gives a value for $\bar{\ell}$ of 35.9×10^{-6} sec.

The small spread in the values of α given in Table 3.14 may be attributed primarily to counting statistics. It appears that the system, including the region beyond the Be reflectors, is rather closely coupled and modal effects do not present a problem when the core is close to critical.

Table 3.14

PULSED NEUTRON RESULTS WITH CORE V NEAR CRITICAL

Probe Location	α (sec^{-1})
g-13	-266.1
k-1	-267.3
g-22	-268.6
Outside Be Reflector	-271.0

The type "N" poison tubes (0.1278 molar) were then replaced with type "M" tubes (0.1704 molar) resulting in a core that was several dollars subcritical. The results obtained from the pulsed-neutron measurements on this core with the detector probe at two locations are compared in Table 3.15 to the results obtained by mapping.

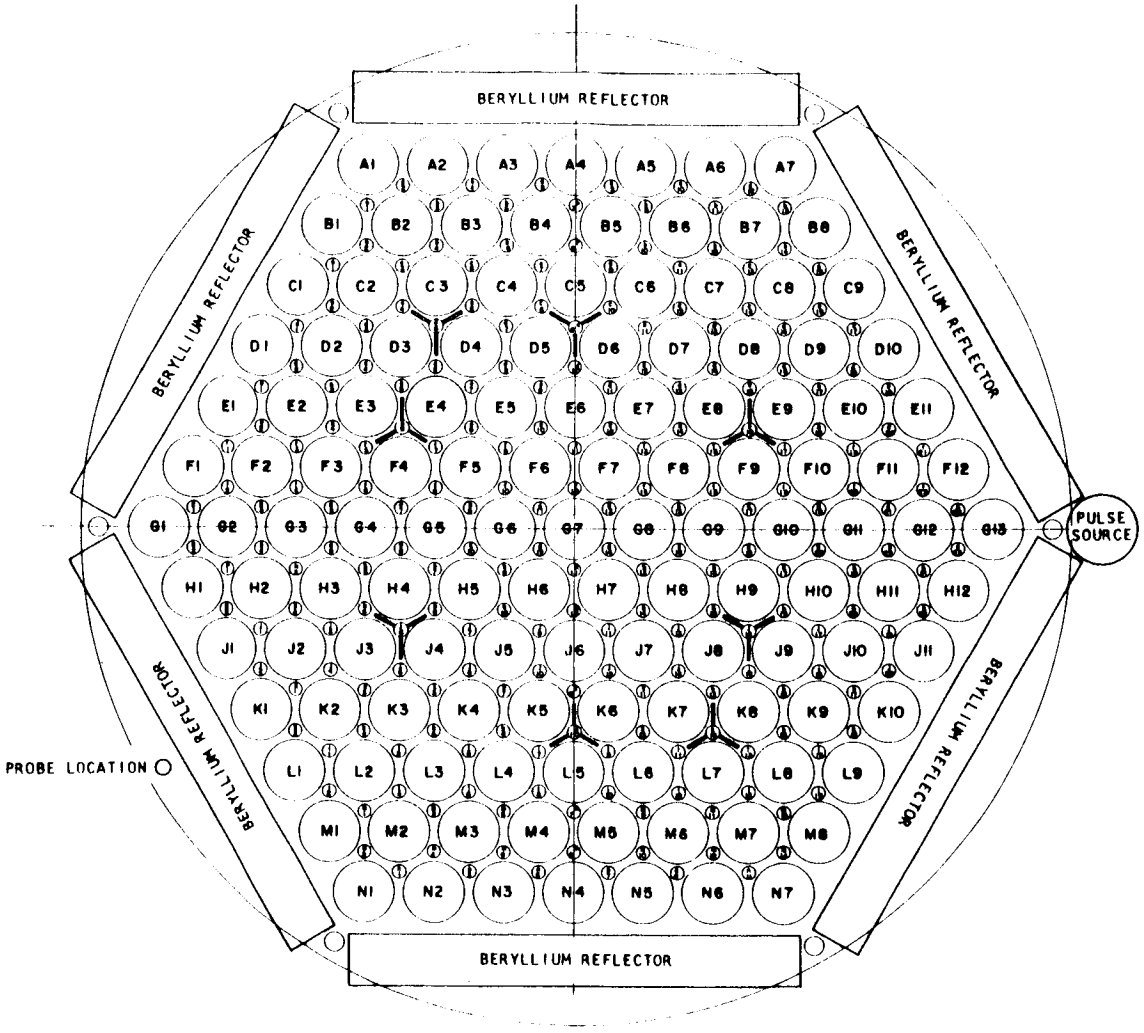

Fig. 3.3--Pulse source and detector probe locations

Table 3.15

PULSED NEUTRON RESULTS WITH TYPE "M" POISON TUBES IN CORE V

Probe Location	$\alpha(\text{sec}^{-1})$	Experimental Reactivity ($)	Standard Core Pulse ($)	Standard Core Mapping ($)
g-13	-694.4	-2.60	-2.50	-2.647
k-1	-726.2	-2.77	-2.63	-2.647

The "Experimental Reactivity" results in Table 3.15 are the values found from the equation:

$$\rho = \frac{1 + \frac{l\alpha}{\beta_{eff}}}{1 + l\alpha} \qquad (3.1)$$

These values must be corrected to account for the absence of poison tubes at the control rod, source tube, and detector locations; the corrected values are shown in Column 4 of Table 3.15 as "Standard Core Pulse." The reactivity values for the standard core found by mapping are shown in Column 5 for comparison.

IV. ANALYTICAL METHODS AND RESULTS

4.1 EIGENVALUE CALCULATIONS

4.1.1 SUMMARY OF THE CALCULATIONS

Refined calculational methods were used for all of the eigenvalue calculations for the zoned cores. These methods and the increase in accuracy associated with their use have been described in detail in Sections IV and VIII of Ref. 1. The calculational scheme may be summarized as follows:

1. High energy disadvantage factors were obtained for all the core components aside from cadmium in a one-dimensional cell transport calculation using GAPLSN.[2] An equivalent Wigner-Seitz cylindrical cell of 4.001 cm radius was used in a P_1-S_8 approximation.

2. Five-group thermal disadvantage factors of all core constituents with the exception of cadmium were obtained in a two-dimensional R-Z transport cell calculation using the DDF code.[3] The fuel stage was explicitly represented, including the 1/8-in. gap between stages. The moderator water was shown as a cylindrical annulus, and the cadmium solution was represented as an outermost annular ring containing the poison volume associated with each cell. Disadvantage factors were determined for cells in each of the regions of the core.

3. The thermal disadvantage factors for cadmium were obtained by interpolation from a series of two-dimensional transport calculations of the hexagonal unit cell. These calculations were described in Section 4.10 of Ref. 1 and use an X-Y plan view representation of the unit hexagonal cell.

4. The resonance calculations for nuclides in each of the core regions were performed using the GAROL[4] code. This treatment allows consideration of resonance overlap as well as specifically taking into account the limited moderator region of the cell.

5. Thermal and fast spectra were computed in the GATHER-II[5] and GAM-II[6] codes respectively, using the disadvantage factors and averaged resonance energy cross sections obtained in the previous steps. Resonance calculations above ~ 1 keV were done in the GAM-II code using the Nordheim integral method. Pointwise microscopic cross sections were averaged over these spectra to obtain self-shielded cross sections for ten broad groups. This group structure is given in Table 4.1. Scattering cross sections for the beryllium reflector were obtained from a bound kernel model.

6. The homogenized core was represented in a GAMBLE[7] two-dimensional diffusion calculation converged to 1.5×10^{-5} in eigenvalue. The outer radial boundary of the boral plate was represented by extrapolation distances obtained from one-dimensional transport calculations; this treatment is discussed in Section 4.12 of Ref. 1.

Table 4.1

TEN-GROUP STRUCTURE FOR EIGENVALUE CALCULATIONS

Group	Energy Range
1	2.73 to 14.9 MeV
2	0.498 to 2.73 MeV
3	0.0674 to 0.498 MeV
4	0.0614 to 67.4 keV
5	2.38 to 61.4 eV
6	0.414 to 2.38 eV
7	0.09 to 0.414 eV
8	0.05 to 0.09 eV
9	0.03 to 0.05 eV
10	0.0 to 0.03 eV

4.1.2 CRITICALITY CALCULATIONS

The critical cadmium loading for Core III, the unzoned Be reflected core, was 0.2202 moles/liter. The addition of natural tungsten for zoning necessitated a corresponding decrease in the cadmium concentration to achieve criticality.

In the precritical analyses of the zoned cores, the above cadmium concentration was decreased to obtain a change in worth equal to the estimated worth of the additional tungsten. The eigenvalue was then determined from a refined calculation using this first estimate of the cadmium loading. This enabled a second estimate to be made, for experimental purposes, of the cadmium loading required to obtain a just critical assembly. For both of the zoned cores, the first estimate of the cadmium concentration differed by less than 10% from the final experimental concentration.

After the critical cadmium concentration was measured, the eigenvalue was recalculated using the experimental cadmium loading. The small change in cadmium disadvantage factors was neglected between the first and second calculations. This introduced a negligible error in the results. In Table 4.2, the calculated reactivities of the zoned cores are compared with experimental values. Schematics of the zoned cores are shown in Figs. 4.1 and 4.2, and homogenized atom densities for all the core and reflector regions are given in Tables 4.3 and 4.4.

Table 4.2

RESULTS OF THE REFINED EIGENVALUE CALCULATIONS FOR THE ZONED CORES WITH CADMIUM

	Cadmium Concentration (moles/liter)	Calculated Eigenvalue	Calculated Reactivity ($)	Experimental Standard Core Reactivity ($)
Core IV	0.1705	1.00103	0.145	1.251
Core V	0.1278	1.00056	0.080	0.136

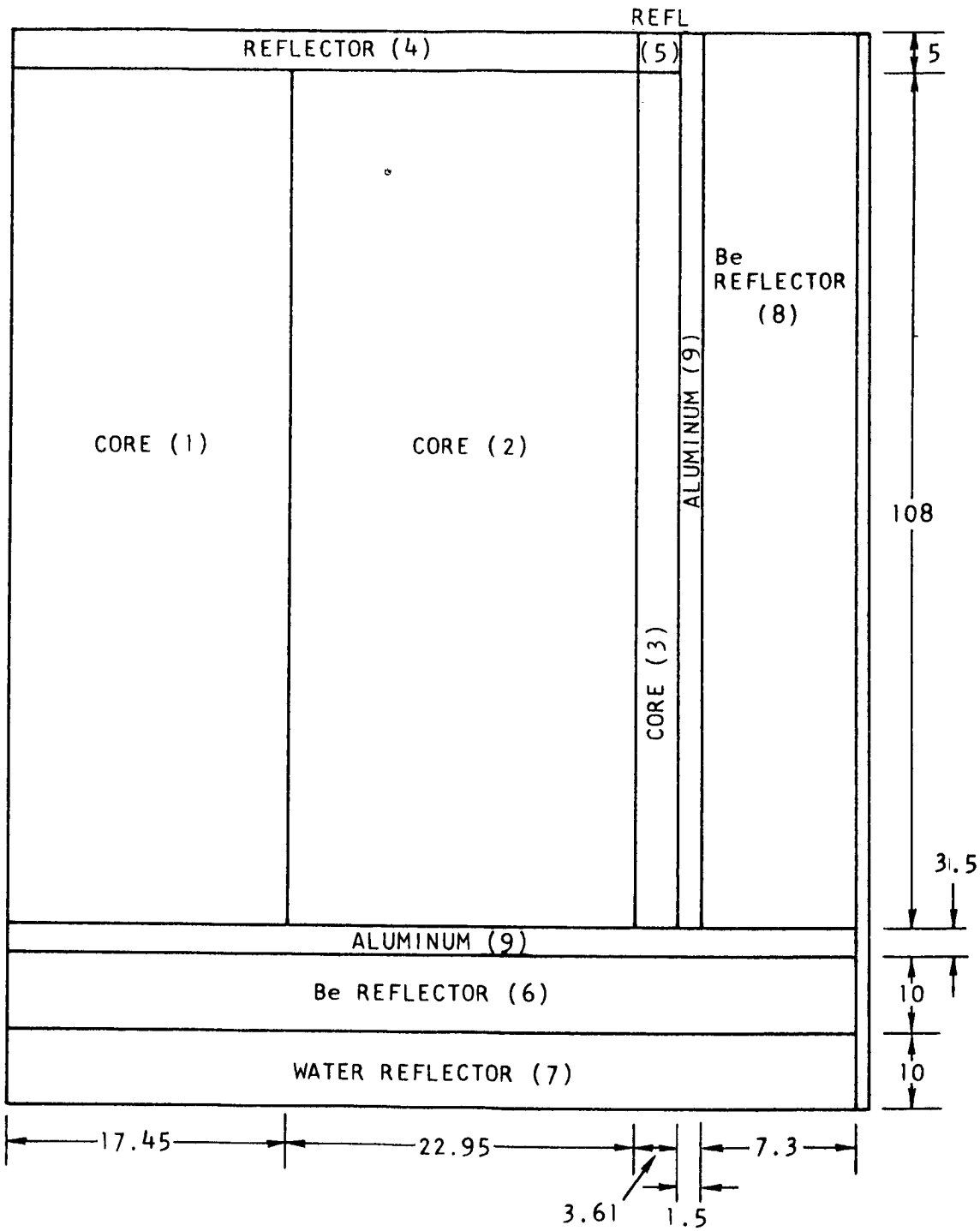

Fig. 4.1--Sketch of radially zoned 3.0-in. pitch assembly, Core IV (dimensions in cm)

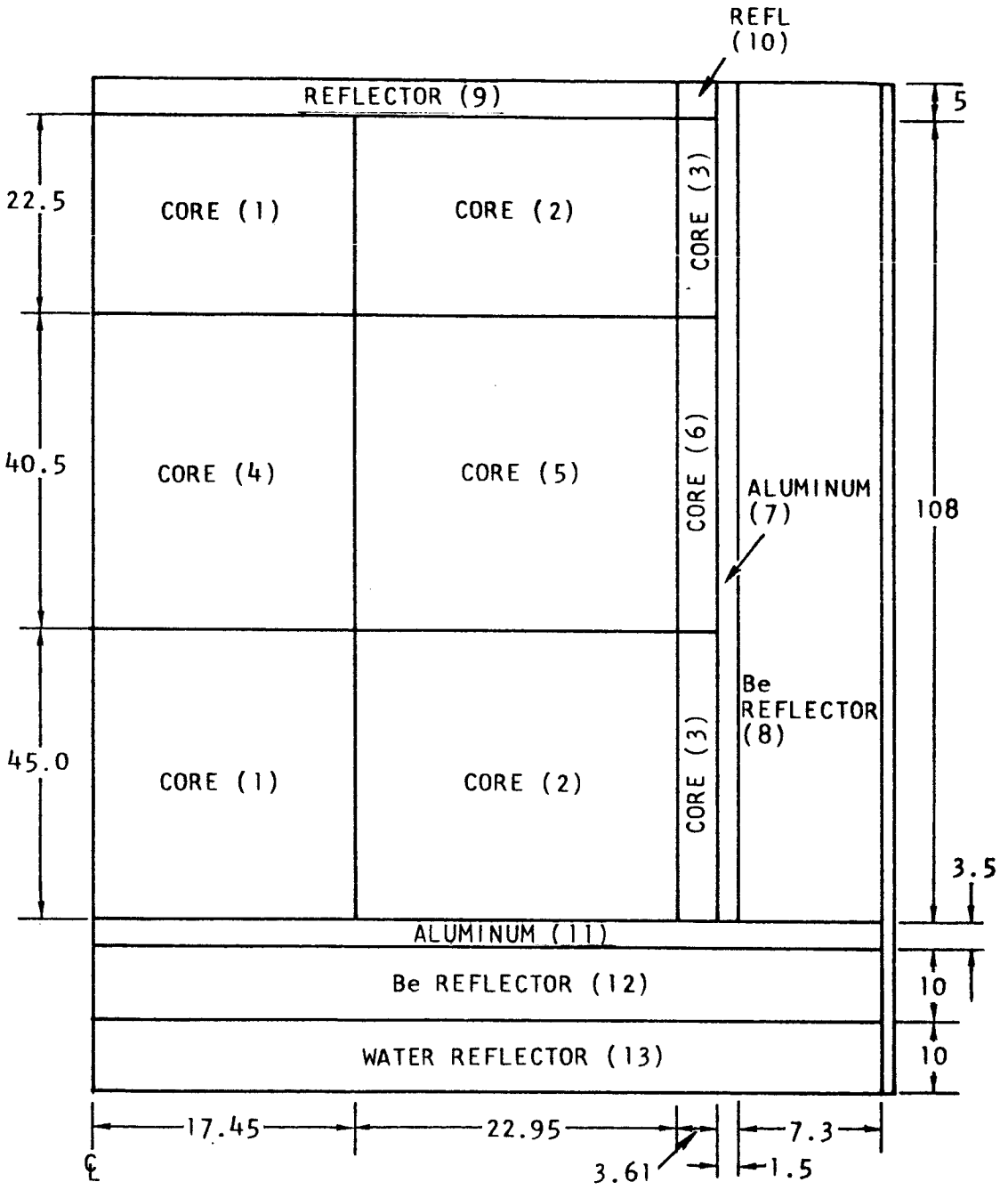

Fig. 4.2--Sketch of fully zoned 3.0-in. pitch assembly, Core V (dimensions in cm)

Table 4.3

HOMOGENIZED ATOM DENSITIES FOR THE RADIALLY ZONED 3.0-IN. PITCH CORE (CORE IV) (atoms/b-cm)

Isotope	Region 1	2	3	4	5	6	7	8	9
H	2.172×10^{-2}	2.172×10^{-2}	2.172×10^{-2}	2.172×10^{-2}	2.172×10^{-2}		6.677×10^{-2}		
O	1.086×10^{-2}	1.086×10^{-2}	1.086×10^{-2}	1.086×10^{-2}	1.086×10^{-2}		3.339×10^{-2}		
Al	1.845×10^{-2}	1.845×10^{-2}	1.845×10^{-2}	8.490×10^{-3}	8.490×10^{-3}				6.020×10^{-2}
N_i	4.4×10^{-5}	4.4×10^{-5}	4.4×10^{-5}						
Zr	9.83×10^{-5}	9.83×10^{-5}	9.83×10^{-5}						
Cd^{113}	6.692×10^{-7}	6.692×10^{-7}	0.0	6.692×10^{-7}	0.0				
W^{182}	3.868×10^{-4}	2.519×10^{-4}	2.519×10^{-4}						
W^{183}	2.104×10^{-4}	1.374×10^{-4}	1.374×10^{-4}						
W^{184}	4.484×10^{-4}	2.92×10^{-4}	2.92×10^{-4}						
W^{186}	4.162×10^{-4}	2.710×10^{-4}	2.710×10^{-4}						
U^{235}	3.735×10^{-4}	3.735×10^{-4}	3.735×10^{-4}						
U^{238}	1.521×10^{-3}	1.521×10^{-3}	1.521×10^{-3}						
Be						1.228×10^{-1}		1.228×10^{-1}	

Table 4.4

HOMOGENIZED ATOM DENSITIES FOR THE FULLY ZONED 3.0-IN. PITCH CORE (CORE V) (atoms/b-cm)

Isotope	Region 1	2	3	4	5	6	7	8	9	10	11	12	13
H	2.172×10^{-2}	2.172×10^{-2}	2.172×10^{-2}	2.172×10^{-2}	2.172×10^{-2}	2.172×10^{-2}			2.172×10^{-2}	2.172×10^{-2}			6.677×10^{-2}
O	1.086×10^{-2}	1.086×10^{-2}	1.086×10^{-2}	1.086×10^{-2}	1.086×10^{-2}	1.086×10^{-2}			1.086×10^{-2}	1.086×10^{-2}			3.339×10^{-2}
Al	1.845×10^{-2}	1.845×10^{-2}	1.845×10^{-2}	1.845×10^{-2}	1.845×10^{-2}	1.845×10^{-2}	6.02×10^{-2}		8.49×10^{-3}	8.49×10^{-3}	6.02×10^{-2}		
Ni	4.4×10^{-5}	4.4×10^{-5}	4.4×10^{-5}	4.4×10^{-5}	4.4×10^{-5}	4.4×10^{-5}							
Zr	9.83×10^{-5}	9.83×10^{-5}	9.83×10^{-5}	9.83×10^{-5}	9.83×10^{-5}	9.83×10^{-5}							
Cd^{113}	4.461×10^{-7}	4.461×10^{-7}	0.0	4.461×10^{-7}	4.461×10^{-7}	0.0			4.461×10^{-7}	0.0			
W^{182}	3.868×10^{-4}	2.519×10^{-4}	2.519×10^{-4}	6.745×10^{-4}	5.396×10^{-4}	5.396×10^{-4}							
W^{183}	2.104×10^{-4}	1.374×10^{-4}	1.374×10^{-4}	3.677×10^{-4}	2.945×10^{-4}	2.947×10^{-4}							
W^{184}	4.484×10^{-4}	2.92×10^{-4}	2.92×10^{-4}	7.818×10^{-4}	6.254×10^{-4}	6.254×10^{-4}							
W^{186}	4.162×10^{-4}	2.71×10^{-4}	2.71×10^{-4}	7.259×10^{-4}	5.807×10^{-4}	5.807×10^{-4}							
U^{235}	3.735×10^{-4}	3.735×10^{-4}	3.735×10^{-4}	3.735×10^{-4}	3.735×10^{-4}	3.735×10^{-4}							
U^{238}	1.521×10^{-3}	1.521×10^{-3}	1.521×10^{-3}	1.521×10^{-3}	1.521×10^{-3}	1.521×10^{-3}							
Be								1.228×10^{-1}				1.228×10^{-1}	

4.1.3 EXCESS REACTIVITY CALCULATIONS

The excess reactivity was experimentally determined by substituting representative poison tubes with water tubes and measuring the resultant change in reactivity. The worths obtained were summed to give the total reactivity available for an unpoisoned core. In each measurement only a few poison tubes were removed at a time; therefore, the spectrum throughout most of the core was primarily a cadmium poisoned spectrum. Thus, in the calculation of the excess reactivity, the best approximation would be to use cross sections which have been averaged over a poisoned spectrum.

The excess reactivity was calculated for the zoned cores by merely setting the cadmium concentration equal to zero in the two-dimensional GAMBLE diffusion calculation and reconverging the original critical problem. By retaining cross sections averaged over the cadmium-poisoned spectrum this method most closely corresponds to the actual conditions under which the experimental measurements were made.

The results are shown in Table 4.5, where the calculated values of excess reactivity are compared with the experimental measurements. A value was also calculated for Core III using the same methods and is compared in Table 4.5 to the experimental measurement from Sec. 3.2.3 of Ref. 1.

Table 4.5

EXCESS REACTIVITIES FOR THE ZONED CORES

	Calculated Excess Reactivity ($)	Measured Excess Reactivity ($)
Core III	19.89	20.55
Core IV	17.34	18.43
Core V	13.92	14.24

4.1.4 WORTH OF 10-MIL TUNGSTEN RINGS USED FOR ZONING CORE IV

The worth of the additional tungsten used for radial zoning in Core IV was calculated by replacing the macroscopic cross sections in the radially zoned region with unzoned cross sections and reconverging the original GAMBLE critical calculation. The calculated worth is compared with the experimental value in Table 4.6.

Table 4.6

WORTH OF 10-MIL TUNGSTEN RINGS IN CORE IV

	Calculated Eigenvalue Radially Zoned 0.1705 Molar Cadmium	Calculated Eigenvalue Unzoned 0.1705 Molar Cadmium	Calculated Removal Worth ($)	Measured Removal Worth ($)
0.00710	1.00103	1.01797	2.34	2.36

4.2 AXIAL AND RADIAL POWER DISTRIBUTIONS

The axial and radial power distributions and isopower plots for both of the zoned cores was calculated in the GAMBLE diffusion code using the refined calculational method summarized in Sec. 4.1.

4.2.1 RADIALLY ZONED CORE - CORE IV

In Fig. 4.3 a radial power traverse in Core IV at a core height of 46 cm is compared with experimental results from Table 3.8. The experimental data have been normalized such that

$$\frac{\int_0^{36.89} \overline{P}(r) 2\pi r\,dr}{\int_0^{36.89} 2\pi r\,dr} = \frac{\sum_i^{85} \frac{P_i}{P_o}}{85} \qquad (4.1)$$

where $\overline{P}(r)$ is the calculated local-to-average power ratio, and P_i/P_o is the normalized experimental value of the ratio of the percent of the total core power in the i^{th} fuel element to that in the average fuel element. The normalization excluded the 36 outer fuel elements because of the poor fit between the calculated and measured power near the core-reflector interface. The 36 outer fuel elements, which all directly face the reflector, are represented in Fig. 4.3 by the outermost four points.

A two-dimensional isopower plot of the radially zoned core is shown in Fig. 4.4. The power flattening effect of the additional tungsten in the center zone may be clearly seen, especially when Fig. 4.4 is compared to Fig. 4.5 which is an isopower plot of the unzoned core.

4.2.2 FULLY ZONED CORE - CORE V

In Figs. 4.6 through 4.11, radial and axial power traverses from a GAMBLE calculation are compared with experimental results from Table 3.10. Radial positions of each of the fuel elements are given in Table 3.10. The experimental traverse for fuel element J-1, which is one of the outermost fuel elements, is compared with calculated values of radii of 44.01 cm and 37.17 cm. This was done because the actual hexagonal core boundary and the cylindrical core boundary used in the calculations do not coincide.

A two-dimensional isopower plot of the fully zoned core is shown in Fig. 4.12. The power shaping effect of the additional tungsten in the axial zone may be clearly seen when Fig. 4.12 is compared to isopower plots of the unzoned and radially zoned cores (Figs. 4.5 and 4.4).

4.3 EFFECTIVE DELAYED NEUTRON FRACTION

The effective delayed neutron fraction, β_{eff}, was computed for the zoned cores using the method of Henry.[8] This method has been described in detail in Sec. 4.13 of Ref. 1. The group structure and

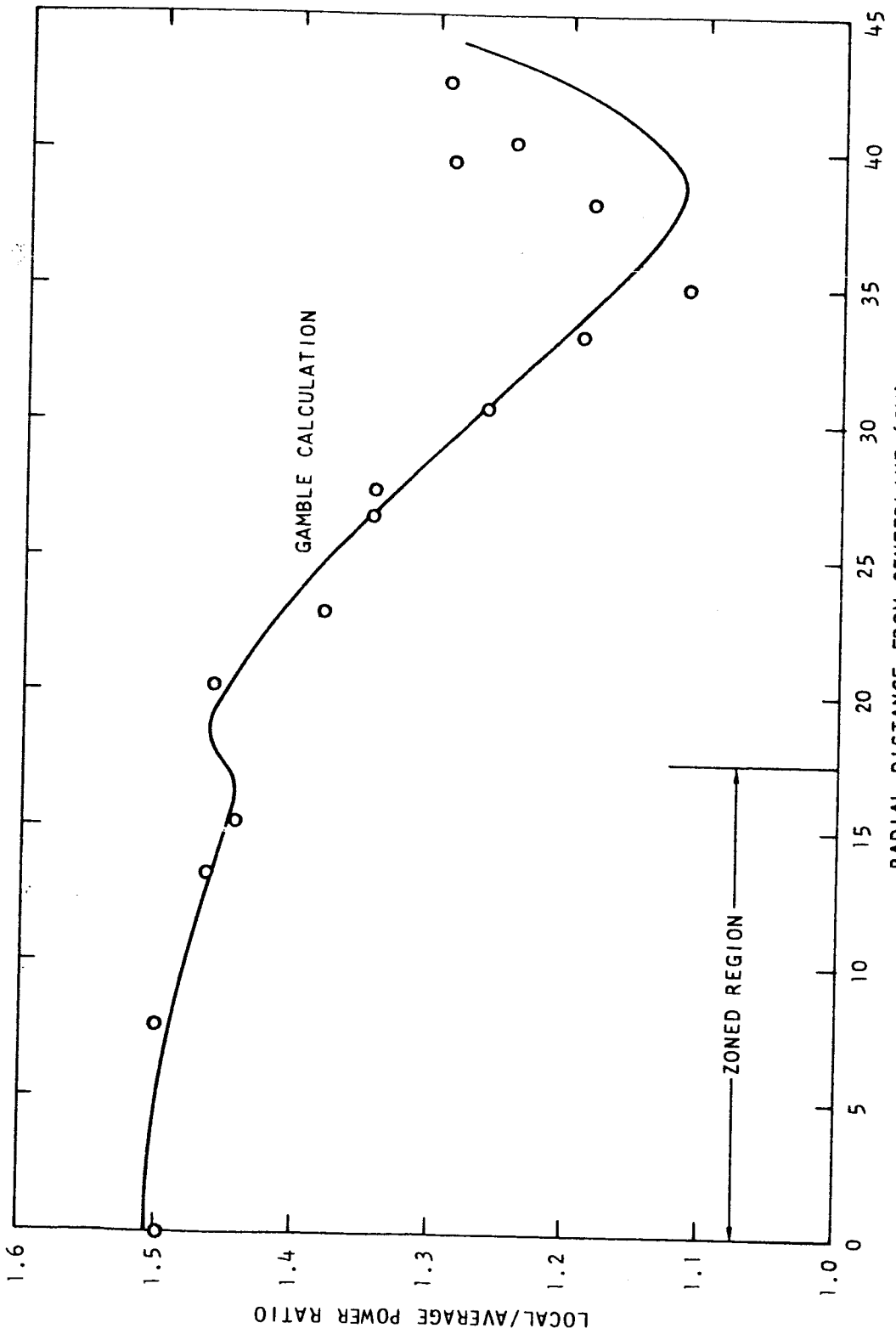

Fig. 4.3--Radial power traverse at core height of 46 cm. Comparison of experimental results with analysis (3.0-in. pitch, Be-reflected, radially zoned, Core IV)

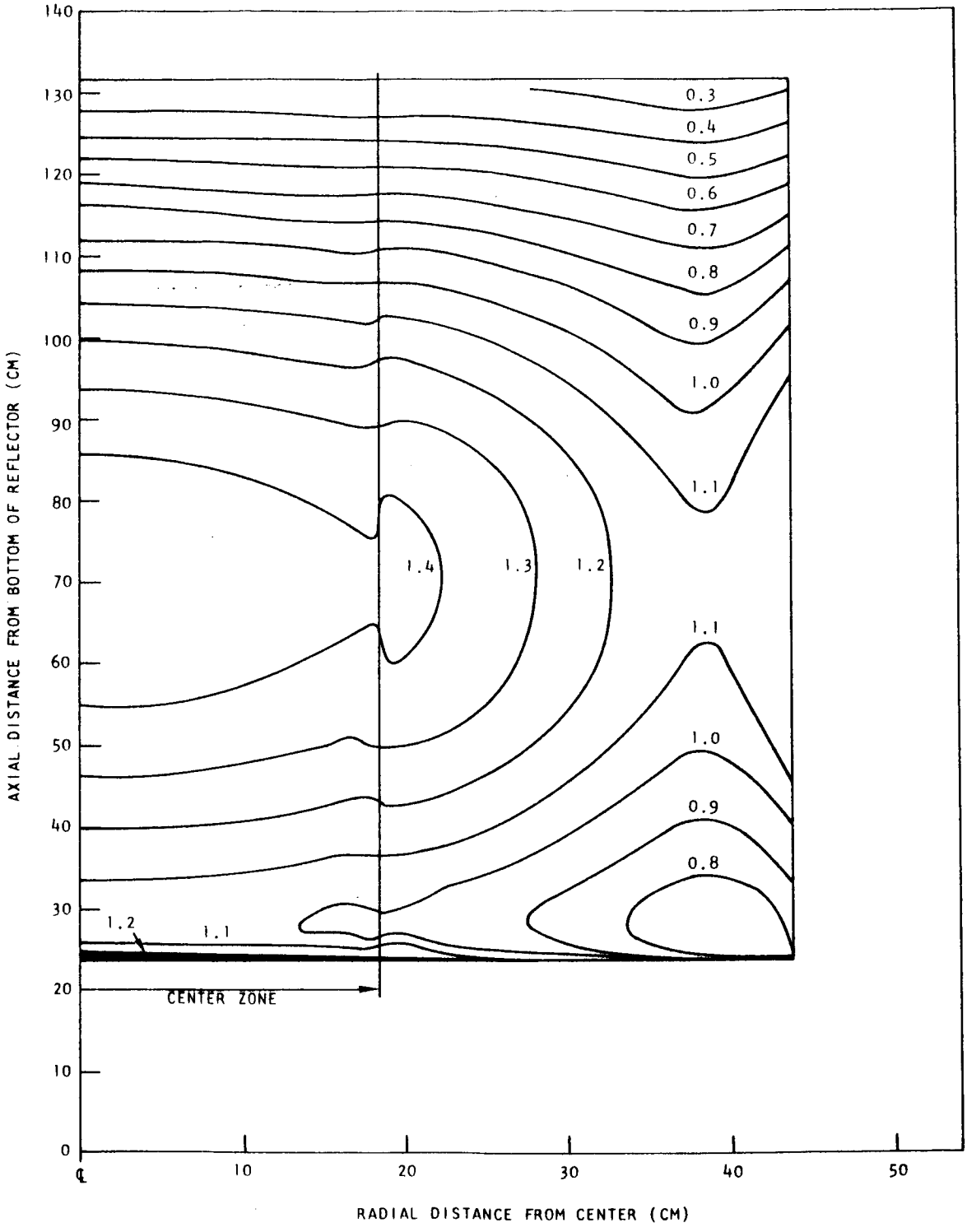

Fig. 4.4--Local/average isopower plot of 3.0-in. pitch radially zoned beryllium-reflected core, Core IV (cadmium = 0.1704 moles/liter)

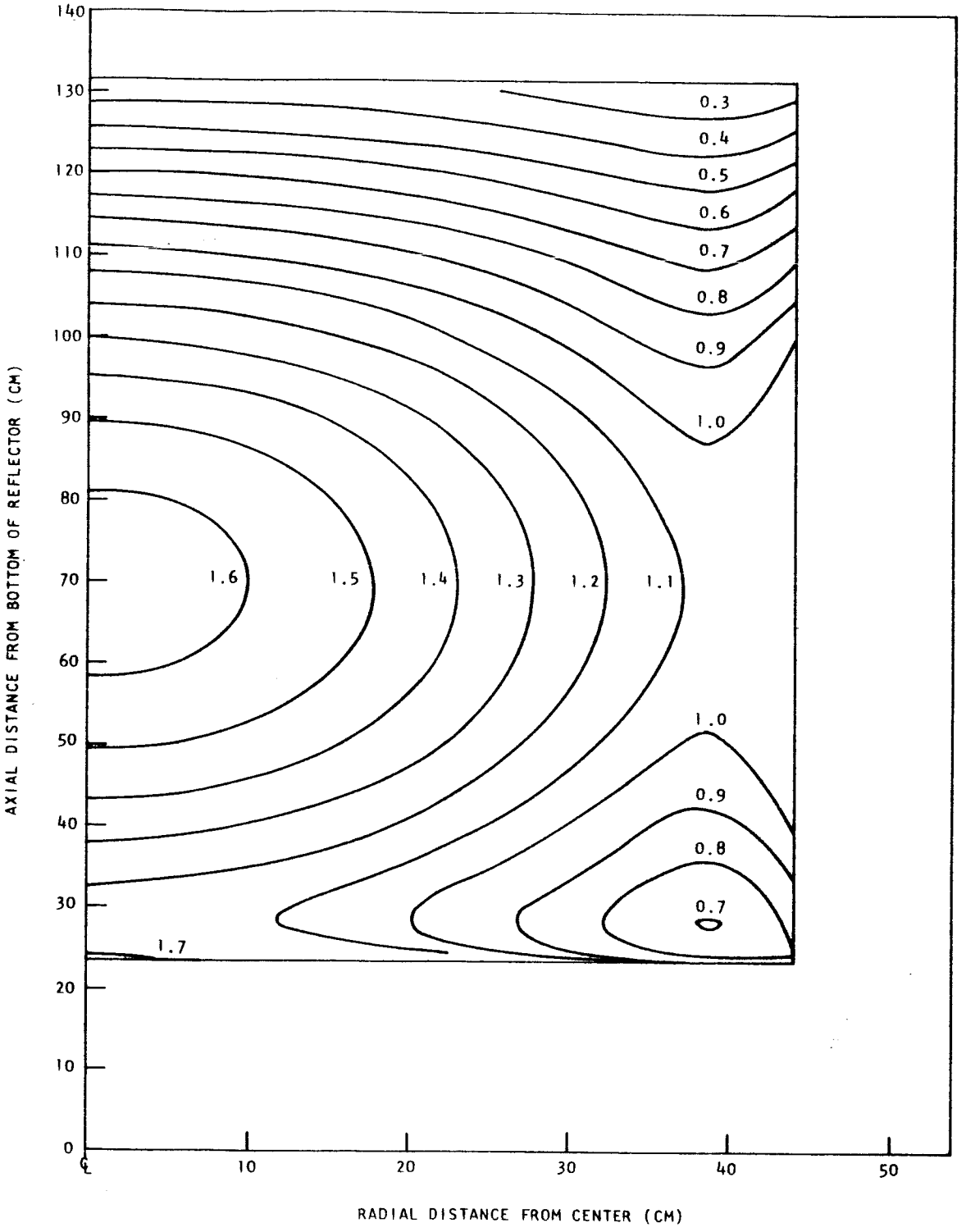

Fig. 4.5--Local/average isopower plot of 3.0-in. pitch, beryllium-reflected core, Core III (cadmium = 0.2202 moles/liter)

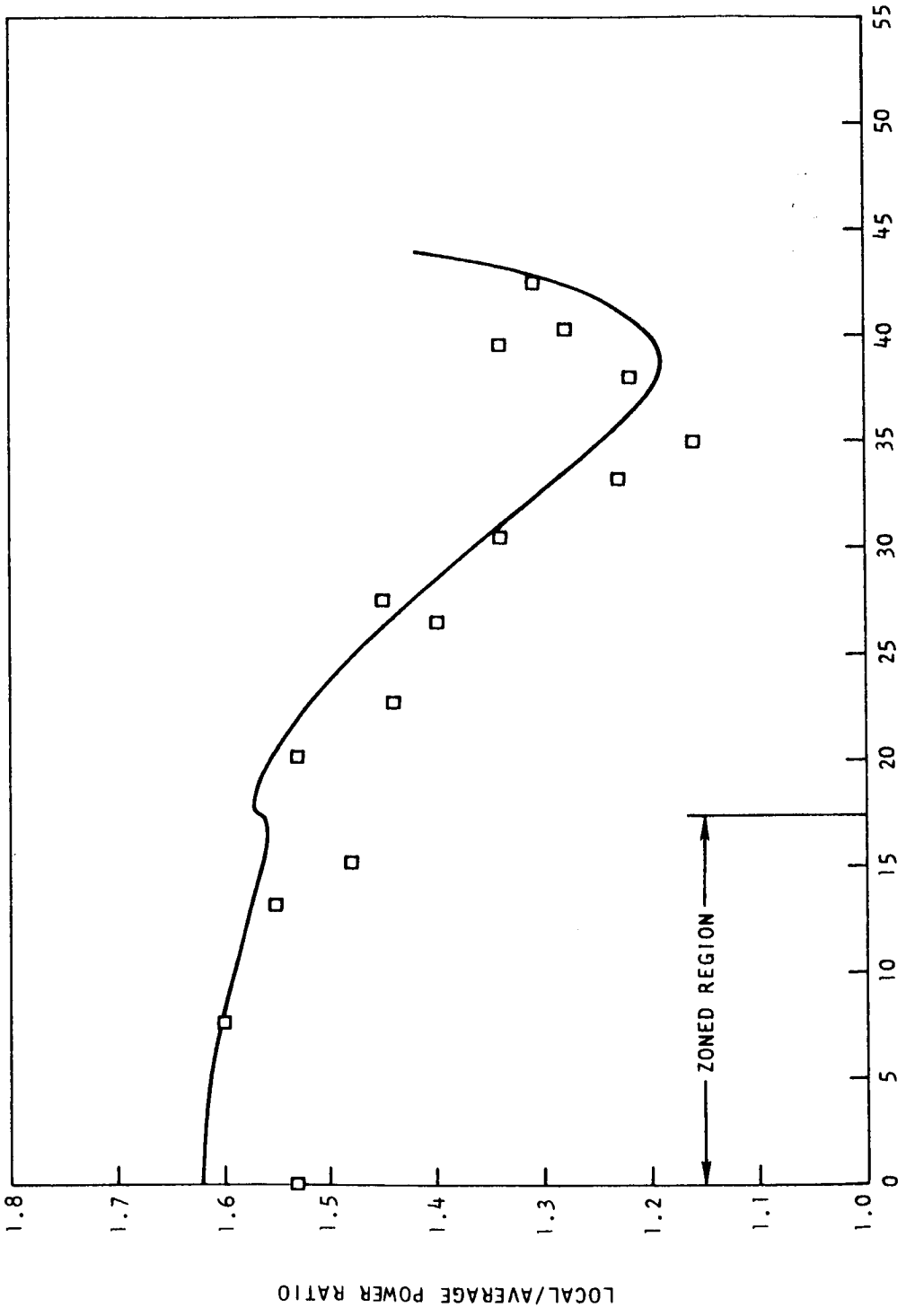

Fig. 4.6--Radial power traverse - Stage 8 comparison of experimental results with analysis (3.0-in. pitch, Be-reflected, fully zoned, Core V)

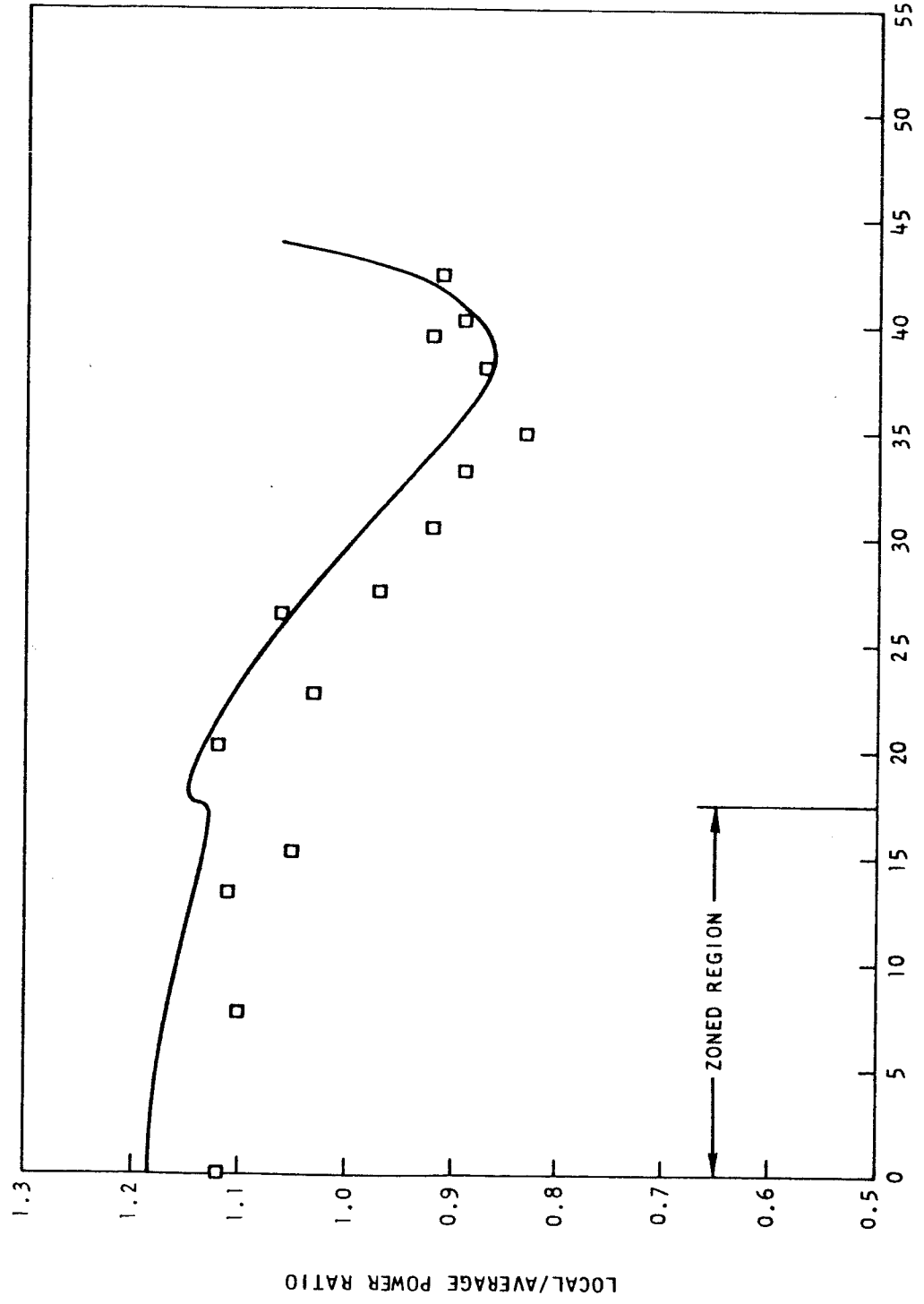

Fig. 4.7--Radial power traverse - Stage 15
comparison of experimental results with analysis
(3.0-in. pitch, Be-reflected, fully zoned, Core V)

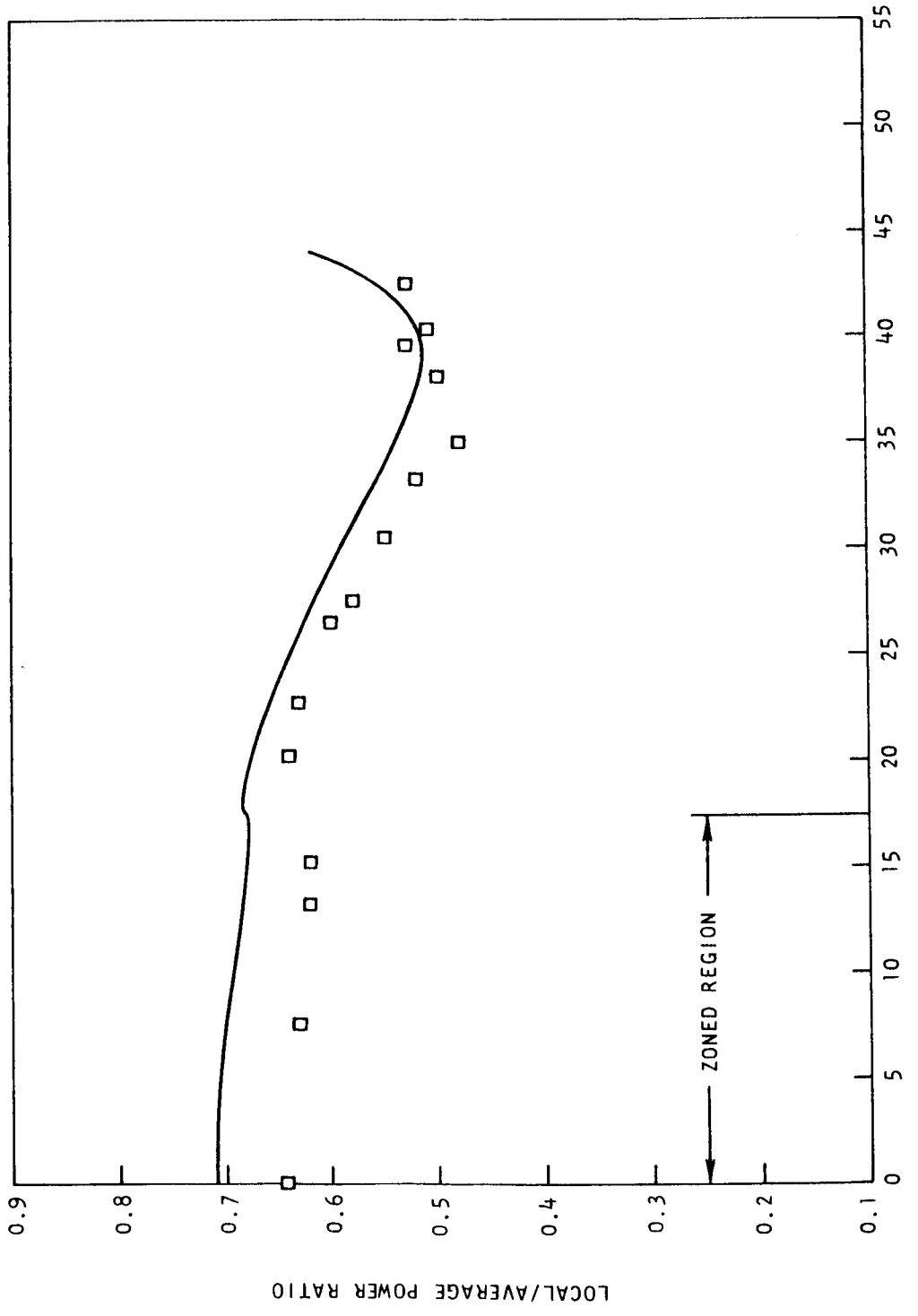

Fig. 4.8--Radial power traverse - Stage 21 comparison of experimental results with analysis (3.0-in. pitch, Be-reflected, fully zoned, Core V)

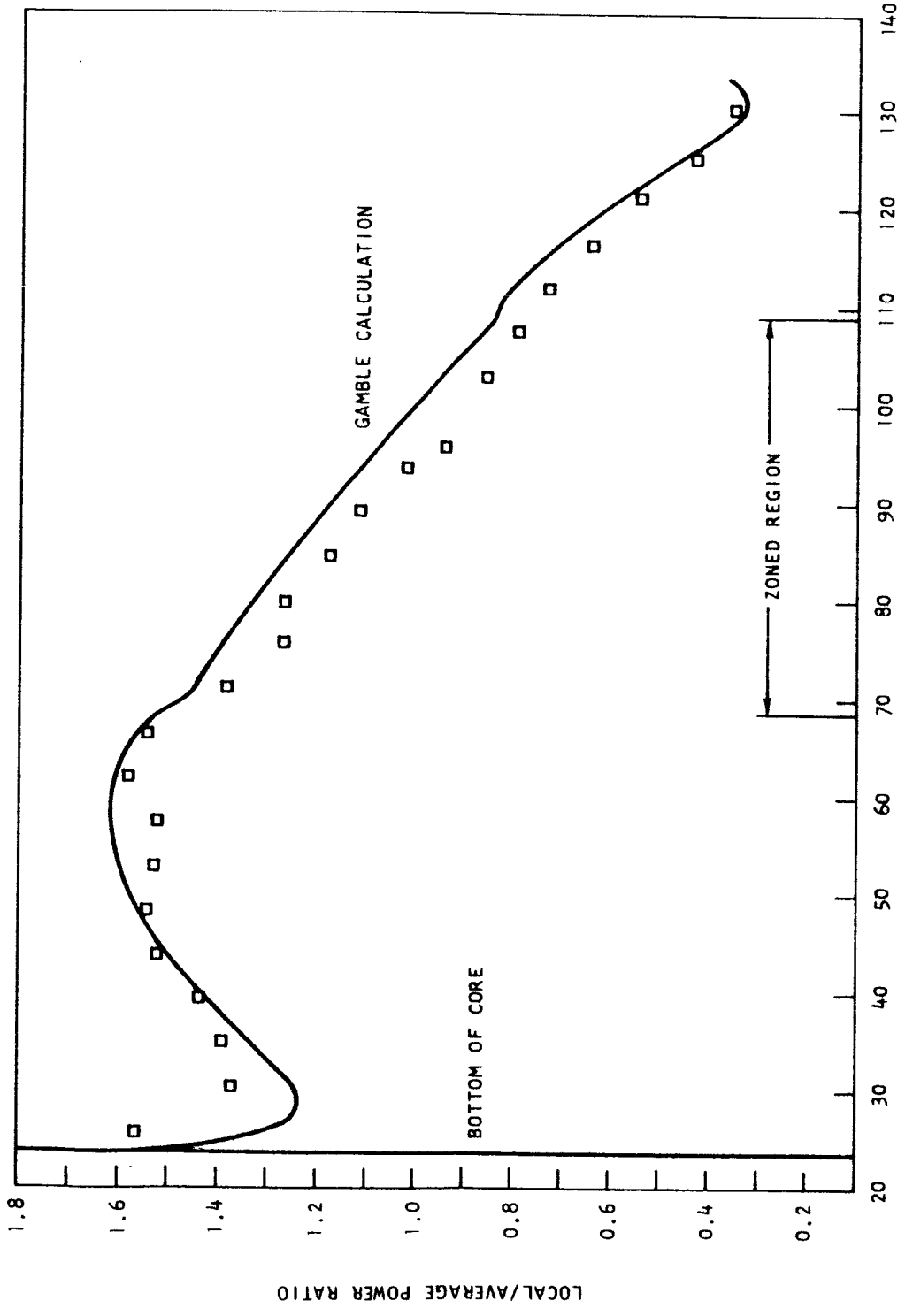

Fig. 4.9--Axial power traverse - fuel element G-7 comparison of experimental results with analysis (3.0-in. pitch, Be-reflected, fully zoned, Core V)

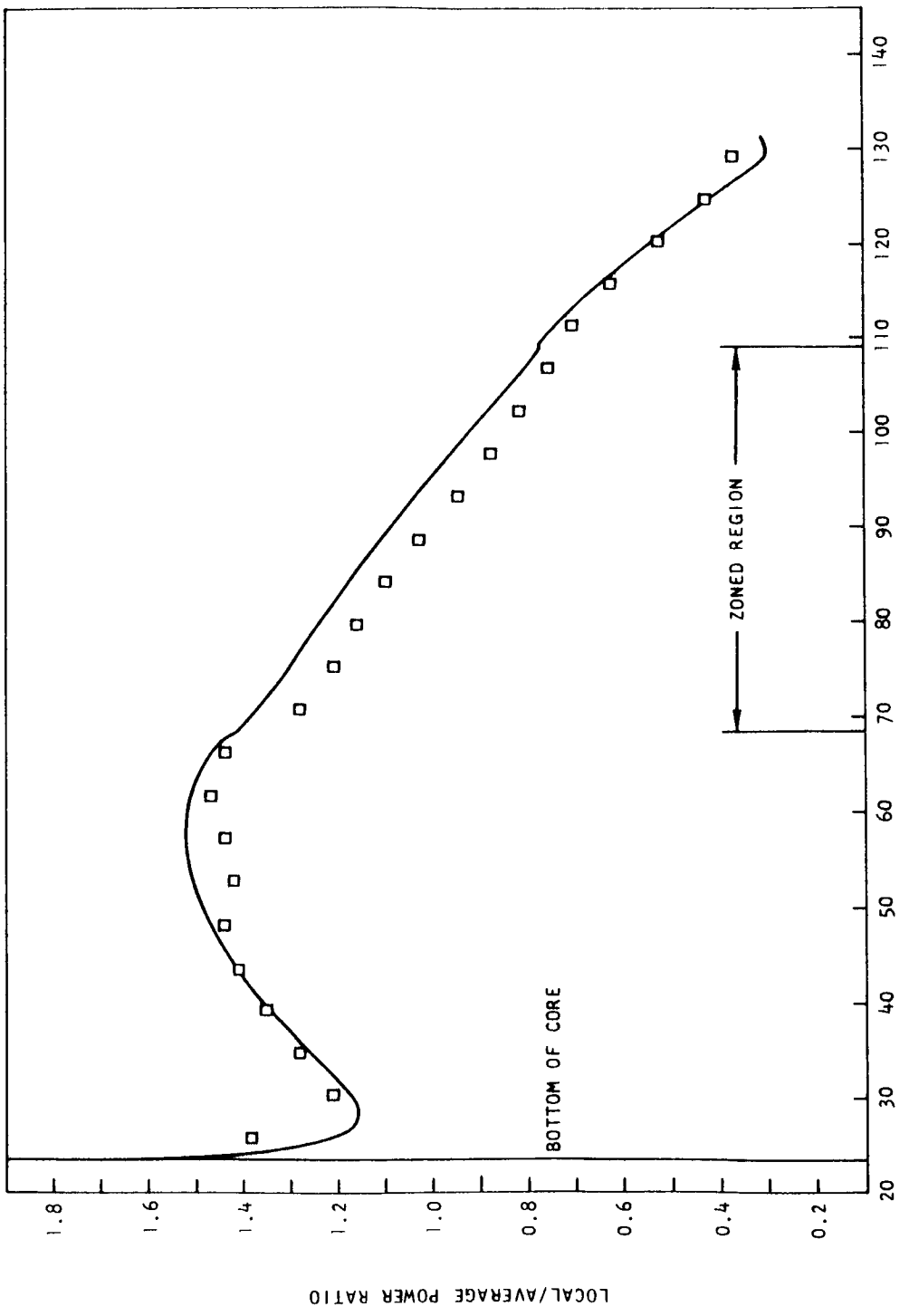

Fig. 4.10--Axial power traverse - fuel element G-4 comparison of experimental results with analysis (3.0-in. pitch, Be-reflected, fully zoned, Core V)

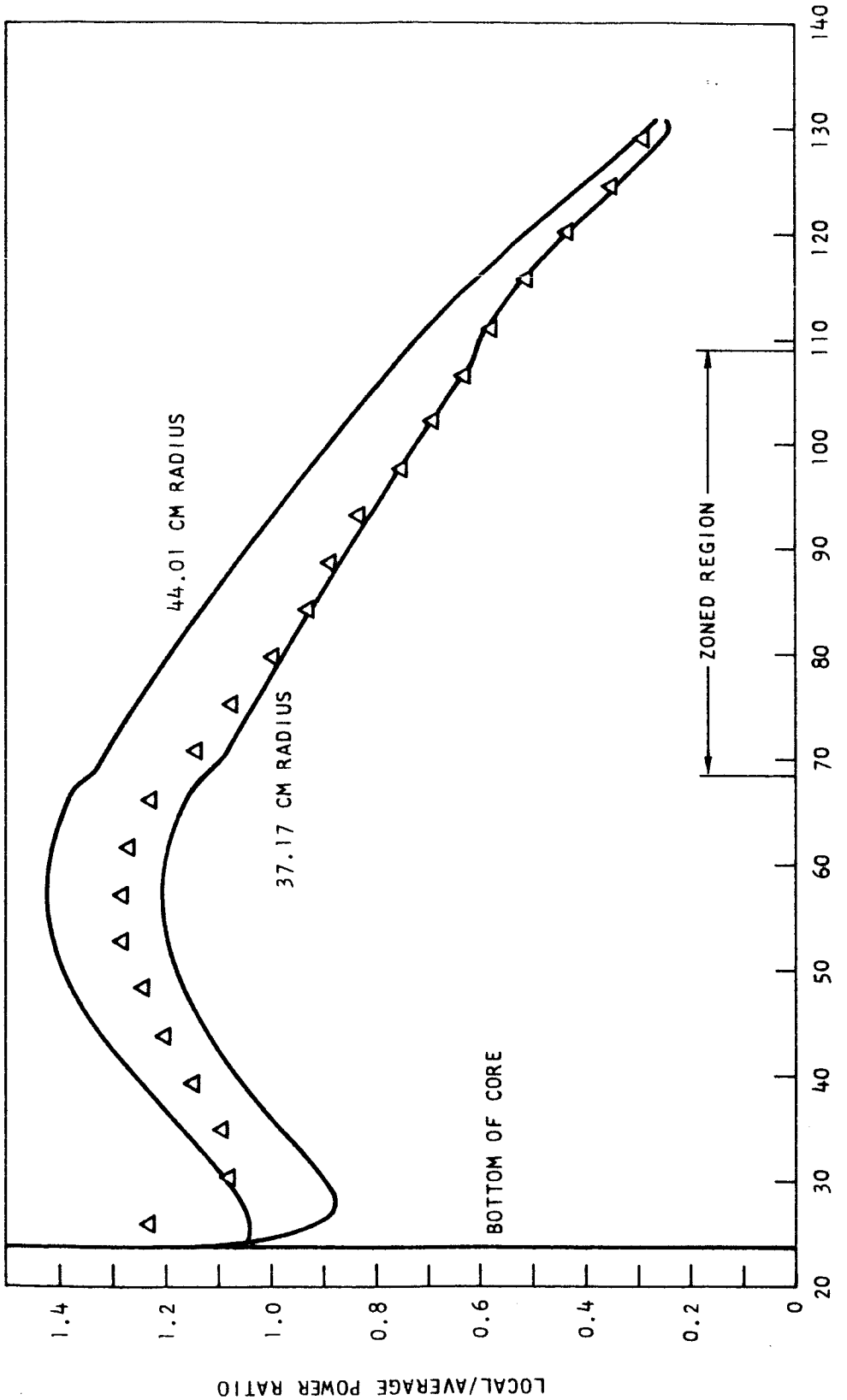

Fig. 4.11--Axial power traverse - fuel element J-1 comparison of experimental results with analysis (3.0-in. pitch, Be-reflected, fully zoned, Core V)

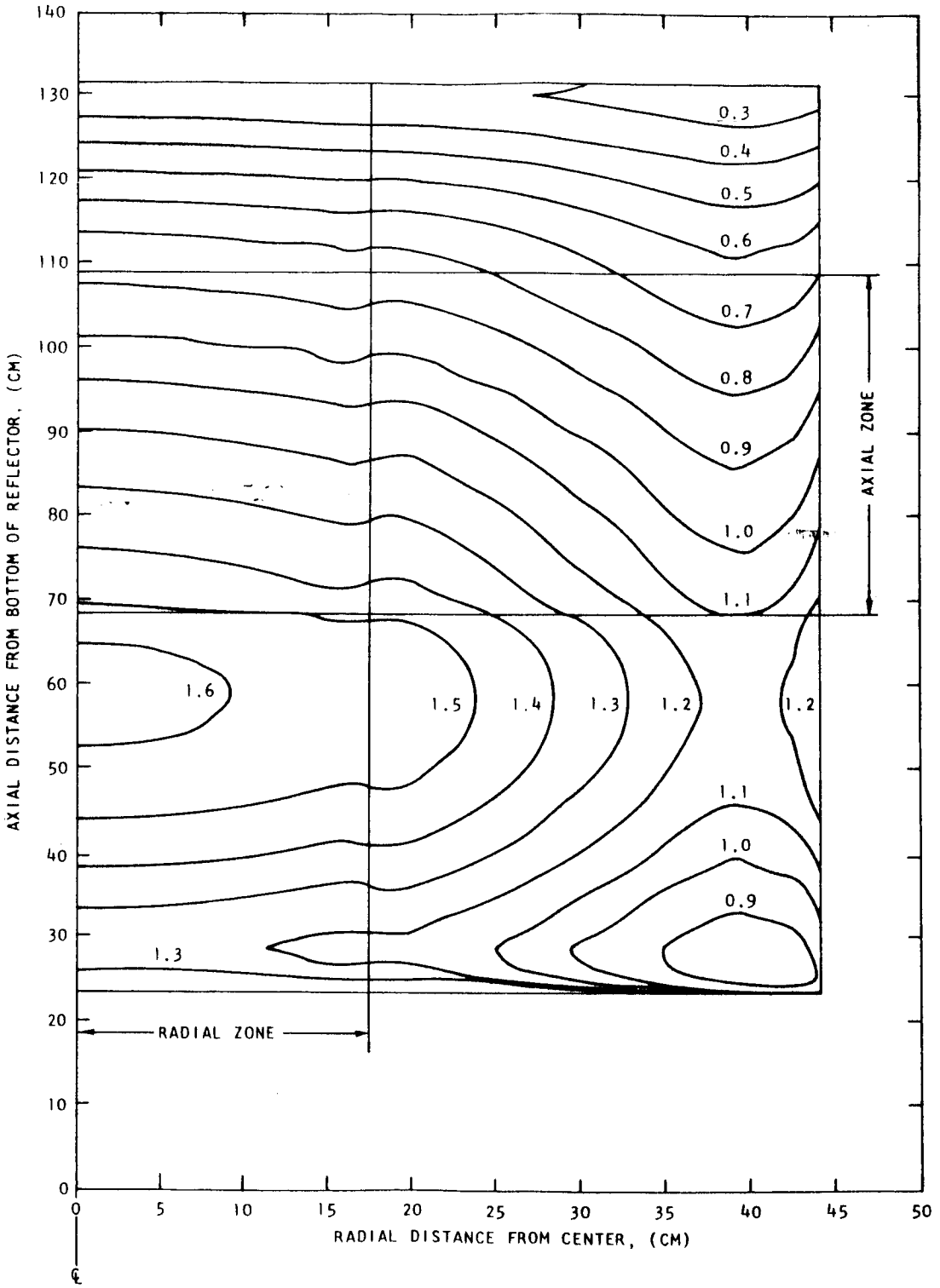

Fig. 4.12--Local/average isopower plot of 3.0-in. pitch fully zoned, beryllium-reflected core, Core V (cadmium = 0.1278 moles/liter)

fission spectrum of Table 4.7 was used. In summary, the initial criticality problem (with the normal fission spectrum) was solved in the GAZE[9] diffusion code using a buckling iteration scheme to account for transverse leakage. The contribution of delayed neutrons to the fission spectrum was then doubled and the problem again solved. The value of β_{eff} was calculated from the relation,

$$\beta_{eff} = \frac{k' - k}{k^2} \qquad (4.2)$$

where k' is the eigenvalue of the perturbed problem and k is the value of the initial criticality problem.

Table 4.7

GROUP STRUCTURE AND NEUTRON SPECTRA FOR β_{eff} CALCULATION

Group		Fission Spectrum $(1 - \beta')f^k$	Delayed Neutron Spectrum $\left\{\sum_i \beta'_i f_i\right\}^k$
1	14.92 to 3.01 MeV	0.20535	0.0
2	3.01 to 1.35 MeV	0.36419	0.00027
3	1.35 to 0.91 MeV	0.14885	0.00079
4	0.91 to 0.41 MeV	0.17507	0.00252
5	0.41 to 0.11 MeV	0.08465	0.00259
6	0.11 MeV to 61.4 eV	0.01527	0.00046
7	61.4 to 2.38 eV	0.0	0.0
8	2.38 to 0.414 eV	0.0	0.0
9	0.414 to 0.09 eV	0.0	0.0
10	0.09 to 0.05 eV	0.0	0.0
11	0.05 to 0.03 eV	0.0	0.0
12	0.03 to 0.0 eV	0.0	0.0

The calculated values of β_{eff} for Cores IV and V were 0.00710 and 0.00703, respectively. Since a consistent method of analysis was used for both cores, the 1% difference may be ascribed to the additional tungsten in the fully zoned core.

4.4 TEMPERATURE COEFFICIENT CALCULATIONS

4.4.1 CALCULATIONAL METHOD

The calculational scheme used to determine the change in reactivity with temperature was similar to that used for the eigenvalue calculations of Sec. 4.1. However, the five thermal-group energy structure was expanded to 18 groups as shown in Table 4.8 and a one-dimensional buckling iteration in the GAZE diffusion code was used to calculate the eigenvalue. Disadvantage factors at 27°C were used in the spectrum calculations for all temperatures. The error associated with the use of a constant set of disadvantage factors and the reasons for the expanded group structure have been discussed in Sec. 6.4 of Ref. 1.

Table 4.8

GROUP STRUCTURE FOR TEMPERATURE COEFFICIENT CALCULATIONS

Group	Energy Range
1	14.9 to 2.7 MeV
2	2.7 to .498 MeV
3	497.9 to 67.4 keV
4	67.4 keV to 61.4 eV
5	61.4 to 2.38 eV
6	2.38 to 1.9 eV
7	1.9 to 1.2 eV
8	1.2 to 1.0 eV
9	1.0 to .6 eV
10	0.6 to 0.414 eV
11	0.414 to 0.33 eV
12	0.33 to 0.23 eV
13	0.23 to .16 eV
14	0.16 to .12 eV
15	0.12 to .09 eV
16	0.09 to .075 eV
17	0.075 to .06 eV
18	0.06 to .05 eV
19	0.05 to .04 eV
20	0.04 to .03 eV
21	0.03 to .02 eV
22	0.02 to .01 eV
23	0.01 to 0.0 eV

The following physical changes were assumed to occur in the assembly with temperature.

1. The water and beryllium density and cadmium concentration decrease with temperature by the reduction factors shown in Table 4.9.

2. The grid plate and axial structural members freely expand with temperature in a linear fashion, according to the formula,

   $\ell(T) = \ell_o(1 + \gamma \Delta T)$, where $\gamma = 2.35 \times 10^{-5} {}^oC^{-1}$ (for aluminum).

The following nuclear changes were accounted for in the calculations:

1. The appropriate hydrogen Nelkin kernel or beryllium crystal kernel was used at each value of the temperature. Accordingly, the free gas kernel for oxygen was computed for the same temperature.

2. Separate resonance calculations for the tungsten isotopes and U^{238} were performed at each value of the temperature.

Table 4.9

WATER AND CADMIUM DENSITY REDUCTION FACTORS

Temperature (^oC)	Density Reduction Factor
27	1.00000
50	0.99198
70	0.98168
100	0.96172

BERYLLIUM DENSITY REDUCTION FACTORS

27	1.000
50	0.9992
70	0.9986
100	0.9976

4.4.2 COMPARISON WITH EXPERIMENT

The reactivity of the 3.0-in. pitch, Be-reflected, fully zoned core (Core V), was calculated as a function of temperature. Four temperatures were used in the calculations: 27°C, 50°C, 70°C, and 100°C.

The results of the calculations are shown in Table 4.10. The reactivity, relative to 27°C, is defined by:

$$\rho(T, 27^{\circ}) = \frac{k(T)-k(27^{\circ})}{\beta_{eff}k(T)k(27^{\circ})} \qquad (4.3)$$

and the temperature coefficient between temperatures T_1 and T_2 is given by:

$$\Delta\rho = \frac{k(T_2)-k(T_1)}{\beta_{eff}k(T_2)k(T_1)[T_2 - T_1]} \qquad (4.4)$$

where $\beta_{eff} = 0.00703$.

Table 4.10

TEMPERATURE COEFFICIENT RESULTS FOR THE 3.0-IN. PITCH, BERYLLIUM-REFLECTED, FULLY ZONED CORE (CORE V)

Temp. (°C)	k_{eff}	$\rho(T, 27^{\circ})$ (cents)	$\Delta\rho$ (cents/°C)
27	0.972797	---	
			- 0.81
50	0.971563	- 18.6	
			- 1.22
70	0.969948	- 43.0	
			- 1.59
100	0.966798	- 90.7	

In Fig. 4.13 the measured reactivity loss is compared with the calculated results. The calculated values do not take into account the change in the thermal disadvantage factors with temperature.

A better understanding of the temperature coefficient can be gained by dissociating the coefficient into its component parts. This has been done in Table 4.11. The usual "generalized five-factor formula" components were computed from the final radial diffusion calculation. The individual components were defined as follows:

$$\eta = \frac{\int_{\text{core}} d^3r \int_0^{2.38\ \text{eV}} dE\,\nu(E)\Sigma_f(\bar{r}, E)\varphi(\bar{r}, E)}{\int_{\text{core}} d^3r \int_0^{2.38\ \text{eV}} dE\,\Sigma_a^{\text{Fuel}}(\bar{r}, E)\varphi(\bar{r}, E)}, \qquad (4.5)$$

$$f = \frac{\int_{\text{core}} d^3r \int_0^{2.38\ \text{eV}} dE\,\Sigma_a^{\text{Fuel}}(\bar{r}, E)\varphi(\bar{r}, E)}{\int_{\text{core}} d^3r \int_0^{2.38\ \text{eV}} dE\,\Sigma_a(\bar{r}, E)\varphi(\bar{r}, E)}, \qquad (4.6)$$

$$\epsilon = \frac{\int_{\text{core}} d^3r \int_0^{\infty} dE\,\nu(E)\Sigma_f(\bar{r}, E)\varphi(\bar{r}, E)}{\int_{\text{core}} d^3r \int_0^{2.38\ \text{eV}} dE\,\nu(E)\Sigma_f(\bar{r}, E)\varphi(\bar{r}, E)}, \qquad (4.7)$$

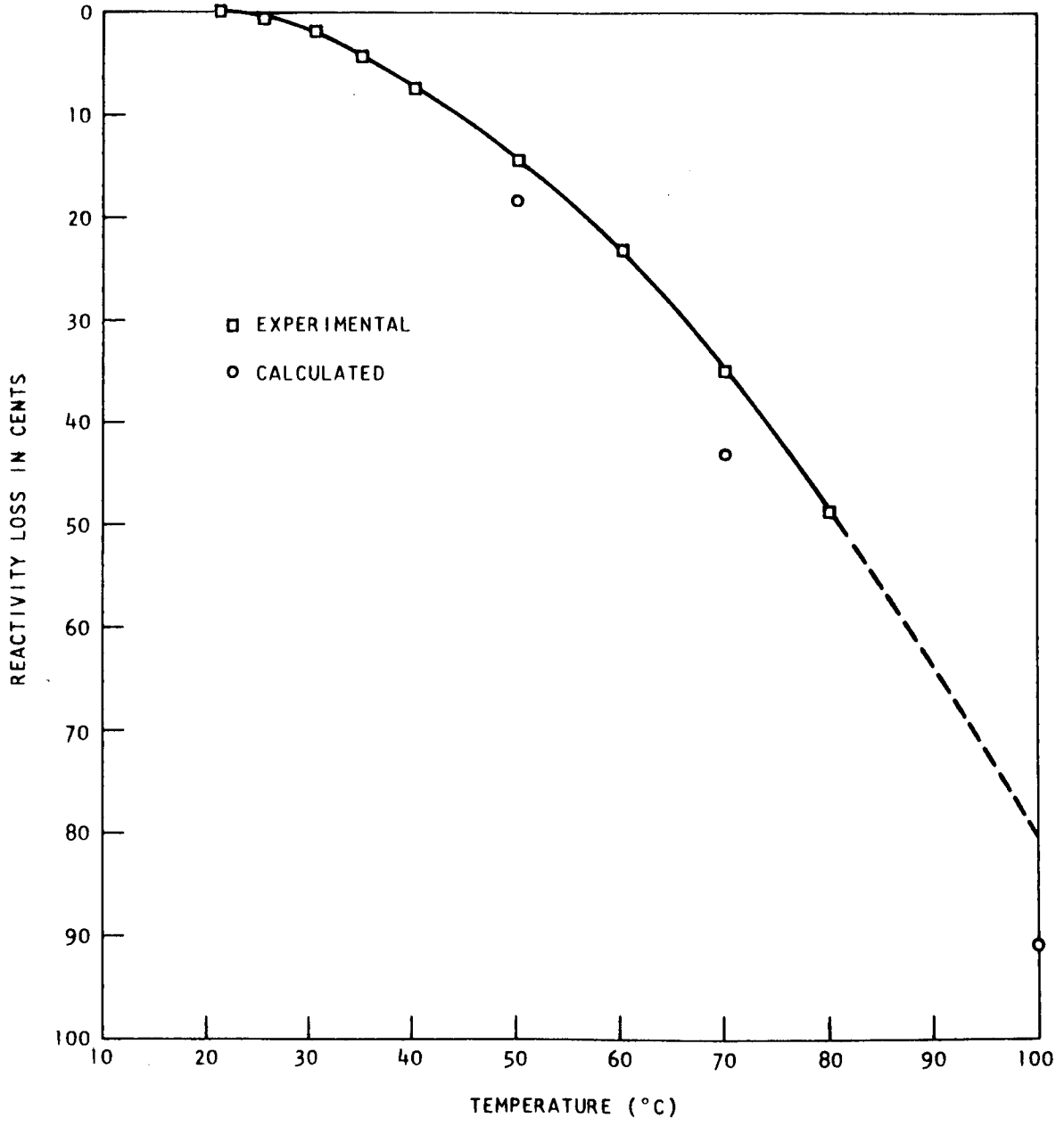

Fig. 4.13--Change of reactivity with temperature, 3.0-in. pitch, Be-reflected, fully zoned core (Core V)

$$p = \frac{\int_{core} d^3r \int_0^{2.38\ eV} dE\Sigma_a(\bar{r}, E)\varphi(\bar{r}, E)}{\int_{core} d^3r \int_0^{\infty} dE\Sigma_a(\bar{r}, E)\varphi(\bar{r}, E)} , \qquad (4.8)$$

and

$$P_{NL} = \frac{\int_{core} d^3r \int_0^{\infty} dE\Sigma_a(\bar{r}, E)\varphi(\bar{r}, E)}{\int_{core} d^3r \int_0^{\infty} dE\Sigma_a(\bar{r}, E)\varphi(\bar{r}, E) - \int_{core} d^3r \int_0^{\infty} dED(\bar{r}, E)\nabla^2\varphi(\bar{r}, E)} . \qquad (4.9)$$

The data in Table 4.11 is discussed in Section 5.4.

4.5 PROMPT NEUTRON LIFETIME

4.5.1 METHOD OF CALCULATION

If a reactor is just critical, the prompt neutron decay time, α_c, is given by the expression,

$$\alpha_c = -\beta_{eff}/\ell , \qquad (4.10)$$

where ℓ is the prompt neutron lifetime for a critical assembly. Equation 4.10 may be derived from a perturbation argument[10] if the prompt neutron lifetime is defined as,

Table 4.11

COMPONENTS OF THE TEMPERATURE COEFFICIENT FOR THE 3.0-IN. PITCH, BERYLLIUM-REFLECTED, FULLY ZONED CORE (CORE V)

Temp. (°C)	η	$\frac{1}{\beta\eta}\frac{\delta\eta}{\delta T}$ (cents/°C)	f	$\frac{1}{\beta f}\frac{\delta f}{\delta T}$ (cents/°C)	ϵ	$\frac{1}{\beta\epsilon}\frac{\delta\epsilon}{\delta T}$ (cents/°C)	p	$\frac{1}{\beta p}\frac{\delta p}{\delta T}$ (cents/°C)	P_{NL}	$\frac{1}{\beta P_{NL}}\frac{\delta P_{NL}}{\delta T}$
27°	2.05510		0.67568		1.38858		0.61155		0.82967	
		- 0.15		1.22		0.95		- 2.06		- 0.72
50°	2.05460		0.67702		1.39070		0.60951		0.82869	
		- 0.19		1.64		1.71		- 3.21		- 1.10
70°	2.05406		0.67858		1.39405		0.60676		0.82742	
		- 0.22		2.05		2.22		- 4.00		- 1.51
100°	2.05310		0.68152		1.40058		0.60163		0.82478	

$$\ell = \frac{\int d^3r \int dE\, \varphi(E, r) v^{-1}(E) \varphi^*(E, r)}{\int d^3r \int dE \varphi(E, r)\, \upsilon\Sigma_f(E, r) \varphi^*(E, r)} , \qquad (4.11)$$

where v^{-1} is the inverse velocity, $\upsilon\Sigma_f$ is the macroscopic neutron production cross section, and φ and φ^* are the scalar and adjoint flux for the critical assembly. The spatial integration is over the entire core and reflector.

Values for α_c are usually calculated for a just critical assembly by finding the amount of 1/v poison removal required to raise the eigenvalue to $1 + \beta_{eff}$. The atom density of the 1/v poison may then be equated to α_c. This method has been discussed in Section 6.5 of Ref. 1; it yields an answer equivalent to Eq. 4.10.

In the calculation of the prompt neutron lifetime, evaluation of Eq. 4.11 is usually inconvenient; however, the method of 1/v poison removal may again be used. In this case a known value of 1/v poison is removed from the entire assembly and the eigenvalue is calculated. The lifetime may then be calculated from the relationship

$$\ell = \frac{\Delta k}{\alpha} , \qquad (4.12)$$

where Δk is the change in eigenvalue produced by a uniformly distributed 1/v absorber with an atom density numerically equal to α. It may be seen that Eq. 4.10 is a particular case of Eq. 4.12 if the lifetime is relatively constant. This may be expected to be the case for calculations of small changes in an assembly close to critical.

4.5.2 COMPARISON WITH EXPERIMENT

A persistent discrepancy between experimental and calculated values of the prompt lifetime has been previously noted in Section 6.5 of Ref. 1. It was postulated that the error might stem from the use of a one-dimensional leakage synthesis; for this reason the prompt lifetime was calculated for Core V using the method described above in a ten-group, two-dimensional GAMBLE diffusion calculation. Two successive GAMBLE calculations, the second of which contained a "1/v" absorber in all the core and reflector regions, were converged to less than 10^{-6} in eigenvalue. The result is compared with the experimental value in Table 4.12. The discrepancy was not resolved by the use of a two-dimensional calculation.

Table 4.12

CALCULATION OF THE PROMPT NEUTRON LIFETIME, CORE V

k	k'	$\alpha(\text{sec}^{-1})$	ℓ_{calc} (μsec)	ℓ_{exp} (μsec)
1.008506	1.012685	-150	27.9	35.9

V. DISCUSSION AND CONCLUSIONS

5.1 EXPERIMENTAL RESULTS NOT ANALYZED

Some of the experimental results given in Section III were not analyzed since previous analysis of similar measurements had shown good agreement.[1] These results include:

1. Safety and regulating rod worths
2. Poison worth as a function of radius
3. Poison worth as a function of concentration.

Several other measurements were not analyzed because of their close similarity to certain measurements which were in good agreement with the analytical results given in Section IV. These include:

1. Worth of 50-mil tungsten added for zoning
2. Worth of tungsten and U^{238} rings in Core IV.

These data, together with those obtained previously are believed to be consistent with analysis and to constitute a complete and well understood body of experimental information on control rod worth, poison rod worth, and fuel element component worth.

5.2 REACTIVITY MEASUREMENTS AND ANALYSIS

5.2.1 CRITICALITY AND EXCESS REACTIVITY

Identical methods were used in the criticality and excess reactivity calculations to find the eigenvalue of the assembly. These methods are summarized in Section 4.1 and have been extensively analyzed in a

previous report.[11] A summary of all the refined calculations of reactivity performed under this contract which could be compared to experimental data is given in Table 5.1.

Table 5.1

SUMMARY OF REFINED EIGENVALUE CALCULATIONS
(3.0-IN. PITCH CORES)

Core	Configuration	Calculated Reactivity ($)	Measured Reactivity ($)	Error ($)
I	Unzoned, Water-reflected[1]	+ 0.78 ± .15	+ 0.15	+0.63 ± .15
III	Unzoned, Be-reflected, no Cadmium	+ 19.89 ± .15	+ 20.55	-0.66 ± .15
IV	Radially zoned, Be-reflected	+ 0.15 ± .15	+ 1.25	-1.07 ± .15
IV	Radially zoned, Be reflected, no Cadmium	+ 17.34 ± .15	+ 18.43	-1.09 ± .15
V	Fully zoned, Be-reflected	+ 0.08 ± .15	+ 0.14	-0.06 ± .15

The ascribed uncertainty of ±$0.15 in Table 5.1 is an allowance for convergence uncertainties in the GAMBLE diffusion calculations.

It can be seen from the error column of Table 5.1 that all of the beryllium-reflected cores have a calculated eigenvalue slightly less than the experimental measurement. Since the error is largest for the Core IV calculations the results suggest that the boundary condition at the boral plate is the main contributor to the error. This is because the ratio of flux to current at the boundary was determined from transport calculations only for Cores III and V. (The values previously determined for Core III were used in the calculations for Core IV.) The good agreement between calculation and experiment generally noted in the six cases

of Table 5.1 further confirm the validity of the refined calculational method. These six cases cover both water- and beryllium-reflected cores, zoned and unzoned cores, and poisoned and unpoisoned cores. It may be concluded that the analysis is in good agreement with experiment over a range of possible core configurations and that future calculations may be done using the same methods with a maximum expected error of less than one dollar of reactivity.

5.2.2 WORTH OF 10-MIL TUNGSTEN RINGS IN CORE IV

The calculation of the removal worth in Core IV of the 10-mil tungsten foils added for radial zoning were in excellent agreement with experiment as shown in Table 4.6. This calculation was primarily concerned with the treatment of resonance absorption in the tungsten; the close agreement further tends to confirm the validity of the method.

5.3 POWER DISTRIBUTIONS AND ANALYSIS

Some scatter of the experimental points may be seen in all of the power traverses. This scatter is probably caused by stage-to-stage differences in the construction of the complex fuel element geometry. Consideration of these differences has led to an assignment of a ±2-1/2% standard deviation for each of the experimental points in Fig. 4.3 and Figs. 4.6 through 4.12.

Radial power distribution measurements made in both Cores IV and V (Figs. 4.3 and 4.6) showed significant deviation from analysis at the core-reflector interface; the discrepancy has been noted in previous cores.[1] These differences arise from the use of a circular boundary in the multigroup diffusion calculations; as noted in Section 4.2, the outermost four points of Figs. 4.3 and 4.6 all directly face the reflector and consequently are in a higher thermal flux than that calculated for the same radius in a homogenized diffusion calculation. These core-reflector interface discrepancies are thus qualitatively understood.

The radial power distribution in Core IV is in good agreement with the calculated results, aside from the outermost row of elements. This agreement is, in part, due to the method of normalization which equated the calculated and measured power of the 85 innermost elements. In Core V, where an "E" ring at every stage position in the assembly was counted, it was possible to independently normalize to the average core power in both the experimental and analytical cases. The results for Core V shown in Figs. 4.6 through 4.11 thus represent entirely independent calculations and measurements. Although differences exist between experiment and analysis of from 5 to 10% in the local/average power the general measured power shapes in both the axial and radial direction are in good agreement with calculations.

It may be concluded that the power density of the fuel elements can be predicted in a zoned core with acceptable accuracy at all points away from the core-reflector interface.

5.4 TEMPERATURE COEFFICIENT

The change of reactivity with temperature predicted by analysis was in good agreement with the experimental measurements. As shown in Fig. 4.13 the calculated temperature coefficient was more negative by about 0.20¢/°C than the measured value over the entire temperature range.

The disadvantage factors were not reevaluated at each temperature and it is of interest to estimate the error associated with assuming them to be constant. In Section 6.4 of Ref. 1 the temperature effect on reactivity was evaluated for an unzoned, water-reflected core; the calculations were done at 100°C both with 27°C disadvantage factors and with disadvantage factors evaluated at 100°C. The negative temperature coefficient with the change in disadvantage factors included was found to be 0.19¢/°C more positive over the 27°-100°C range. This difference is almost identical to the previous noted discrepancy of 0.20¢/°C and, if applicable to the beryllium-reflected zoned core, would virtually eliminate any difference between analysis and experiment.

The "five-factor" breakdown of the temperature coefficient of Table 4.11 may be compared to a similar analysis for the unzoned cores in Section 6.4 of Ref. 1. The comparison shows that the relative importance of the components of the temperature coefficient are only slightly changed when tungsten is added for zoning in a beryllium-reflected core.

The large magnitude of most of the components of the temperature coefficient can be seen in Table 4.11. In fact, barring η, each component is greater than or approximately equal to the net effect given in Table 4.11. The fast components, ϵ and p, are large for this core. The magnitude of the fast absorption effect, $\frac{\delta p}{p}$, is greater than the leakage effect, $\frac{\delta P_{NL}}{P_{NL}}$. (It should be recalled that greater than 30% of the fissions in this core are epithermal.)

Clearly, each component of the temperature coefficient is of first order importance, precluding a separable treatment of the over-all coefficient. The complexity of this core necessitates an arduous and careful calculation of the temperature coefficient, with particular care exercised in the treatment of the thermal disadvantage factors.

It may be concluded that the temperature dependence of the core is well understood in the range investigated up to 100°C, and that the temperature coefficient can be predicted with reasonable accuracy using the methods of Section 4.4.

5.5 PROMPT NEUTRON LIFETIME

A persistent discrepancy previously noted in the prompt neutron lifetime[1] was investigated in the fully zoned Core V. The experimental measurement of α, the asymptotic prompt neutron decay constant, was made at several different locations to check for modal interference. The good agreement of the experimental results (Table 3.14) from different detector locations eliminates the possibility that the decay constants measured were not of the primary mode.

It was also postulated in Ref. 1 that the use of a two-dimensional calculation might eliminate the discrepancy. The results of Section 4.5.2 show however, that the value of the prompt neutron lifetime inferred from the calculation is still low by about 20%, slightly worse than that obtained previously with one-dimensional calculations.

The difference between the measured and calculated values of the prompt neutron lifetime (and thus the asymptotic decay constant) is the only significant discrepancy left unresolved. The experimental values are preferred. The discrepancy has no particular bearing on the question of feasibility.

APPENDIX A

CALCULATION OF THE ESCAPE PROBABILITY IN LUMPS OF VARYING ABSORBER CONCENTRATION

by

J. C. Peak

CALCULATION OF THE ESCAPE PROBABILITY IN LUMPS OF VARYING ABSORBER CONCENTRATION

The use of differing enrichments of tungsten in the zoned reference core gives rise to unit cells in which the resonance absorber concentration may vary widely from cylinder to cylinder. This variation of the resonance absorber concentration from one cylinder to another in a unit cell was not a factor in the mockup cell or in the previous unzoned reference cell; in these cases, which were composed of natural and enriched tungsten respectively, the distribution of each tungsten isotope was virtually uniform from cylinder to cylinder.

In the simulation study of the zoned reference core described in Part 2 of this report, it was assumed that the calculational approach used for resonance absorption in the unzoned core could be applied without modification. Thus, the lumped nuclear density was defined to be

$$\bar{N} = \frac{\sum_i N_i V_i}{\sum_i V_i} , \qquad (1)$$

where N_i is the resonance absorber atom density and V_i is the volume of Cylinder i. The mean chord length was defined as

$$\bar{\ell} = 2\bar{a} = \frac{4\sum_i V_i}{S} , \qquad (2)$$

where S is the outermost perimeter of the set of tungsten cylinders. It was further assumed that the collision escape probability function, P_o, could be adequately approximated for the complex nested cylindrical geometry by using the P_o function for a simple homogeneous cylinder with the provision that the lumped nuclear density and mean chord length be defined as in Eqs. (1) and (2). The use of these collision escape probabilities for a homogeneous cylinder is the assumption which is of interest here.

Values of the collision escape probability can be calculated directly for most nonstandard geometries using a one-group solution of the transport equation. Such a calculation of the collision escape probability is made by using a unit cell in which the only material present is the resonance absorber. The source is distributed across the absorber and a one-group calculation is performed in which absorption in the resonance absorber is the only allowed event. The collision escape probability is, then, just the ratio of the neutrons which escape the lump to the total born in the lump, and is a function of the absorption cross section used in the calculation.

For calculations using the GAM-II code, the collision escape probability must fulfill a reciprocity requirement. This requirement is

$$P_{1\to 2} V_1 \Sigma_1 = P_{2\to 1} V_2 \Sigma_2 \,, \tag{3}$$

where subscript 1 refers to the fuel region, subscript 2 refers to the moderator region, V and Σ are the volume and total cross section respectively, and $P_{1\to 2}$ is the escape probability from Region 1 to 2. The relationship of Eq. (3) will be fulfilled for a homogeneous fuel region if the function $P_{1\to 2}$ is calculated using a flat source across the fuel region. In the case where the atom density of the absorber varies within the fuel region however, a flat source is inappropriate. The correct source for the calculation may be derived from the following argument, which is an extension of the flat source derivation of Ref. 1.

Let $G(x, x')$ be the flux at point x in the moderator due to a unit isotropic source at x' in the fuel. Then the reciprocity theorem[2] states that

$$G(x, x') = G(x', x), \tag{4}$$

In a two-region problem the collision rate in the moderator caused by neutrons from a distributed source in the fuel is

$$\int_{V_2} \Sigma_2 \varphi(x) d^3x = \int_{V_2} d^3x \int_{V_1} d^3x' \Sigma_2(x) S_1(x') G(x, x') \tag{5}$$

The escape probability from Region 1 to 2 is the ratio of collisions in Region 2 to the total source in Region 1, or

$$P_{1\to 2} = \frac{\int_{V_2} d^3x \int_{V_1} d^3x' \Sigma_2(x) S_1(x') G(x, x')}{\int_{V_1} S_1(x') d^3x'} \tag{6}$$

From similar considerations it may be seen that

$$P_{2\to 1} = \frac{\int_{V_1} d^3x' \int_{V_2} d^3x \Sigma_1(x') S_2(x) G(x', x)}{\int_{V_2} S_2(x) d^3x} \tag{7}$$

Now $S_2(x)$ and $\Sigma_2(x)$ may be assumed to be constant across the moderator region. Applying the reciprocity theorem, interchanging the order of integration, and removing S_2 and Σ_2 from under the integrals leads to the following equations,

$$P_{1\to 2} = \frac{\Sigma_2 \int_{V_2} d^3x \int_{V_1} d^3x' S_1(x') G(x, x')}{\int_{V_1} S_1(x') d^3x'} \tag{8}$$

and,

$$P_{2\to 1} = \frac{1}{V_2} \int_{V_2} d^3x \int_{V_1} d^3x' \Sigma_1(x') G(x, x'). \tag{9}$$

If the source in Region 1 is distributed in direct proportion to the atom density in Region 1; i.e.,

$$S_1(x') = k\Sigma_1(x') \tag{10}$$

where k is an arbitrary constant, the double integrals in Eqs. (8) and (9) are identical and

$$P_{2\to 1} V_2 \Sigma_2 = P_{1\to 2} V_1 \left[\frac{\int_{V_1} \Sigma_1(x') d^3x'}{V_1} \right]. \tag{11}$$

or

$$P_{2\to 1} V_2 \Sigma_2 = P_{1\to 2} V_1 \bar{\Sigma}_1 . \tag{12}$$

Thus the reciprocity relationship can be maintained if the source used for the calculation of escape probability is distributed in proportion to the atom density in the fuel and if the volume-weighted atom density is used in Eq. (3).

The W^{182} distribution in Zone 3 of the reference zoned core was chosen as an extreme example of varying distribution across the cell. In Zone 3 (the radially zoned region) the W^{182} atom density is quite low in

the parts of the cell, however, the W^{182} atom density is about 20 times higher. A complete physical description of the ring structure in the reference cell is given in Part 2 of this report.

The calculated escape probabilities for the Zone 3 distribution of W^{182} are compared to values for a homogeneous cylinder[2] in Table 1.

Table 1

COMPARISON OF COLLISION ESCAPE PROBABILITIES FOR W^{182}

$\Sigma\bar{a}$	P_o(Calculated)	P_o(Homogeneous)
0.02	0.9767	0.9744
0.10	0.8921	0.8850
0.40	0.6629	0.6516
0.70	0.5178	0.5057
1.50	0.3117	0.3016
5.00	0.1014	0.0992
10.00	0.0507	0.0499

The data in Table 1 show that the escape probability function for a homogeneous cylinder is within 2-3% of the actual values for the particular case of W^{182} in Zone 3 of the reference core. Since this was one of the worst cases from the viewpoint of uniform distribution it is believed that the use of escape probability for an equivalent homogeneous cylinder is an entirely adequate approximation.

REFERENCES

1. C. A. Stevens and C. V. Smith, "GAROL, A Computer Program for Evaluating Resonance Absorption Including Resonance Overlap," General Atomic Report GA-6637, Aug. 1965.

2. K. M. Case, F. de Hoffmann, and G. Placzek, Introduction to the Theory of Neutron Diffusion, Vol. 1, U.S. Government Printing Office, June 1953.

APPENDIX B

AN IMPROVED TREATMENT OF SCATTERING RESONANCES IN SLAB GEOMETRY

by

Sanford C. Cohen

GENERAL ATOMIC

DIVISION OF

GENERAL DYNAMICS

JOHN JAY HOPKINS LABORATORY FOR PURE AND APPLIED SCIENCE

P.O. BOX 608, SAN DIEGO, CALIFORNIA 92112

GA-7144

AN IMPROVED TREATMENT OF SCATTERING RESONANCES IN SLAB GEOMETRY

by

Sanford C. Cohen

Submitted for Publication as
a Technical Note in Nuclear
Science and Engineering

SNPC-27

May 13, 1966

Modern computer techniques for the calculation of resonance integrals in heterogeneous geometries are generally quite effective.[1] One of the principle limitations, however, is the flat source assumption used in computing collision probabilities. For heavily absorbing resonances this assumption poses no serious difficulties, but resonances with large scattering components may lead to significant errors. The discrepancy between analysis and experiment in the recent measurement of the W^{186} resonance integral has been attributed in part to this difficulty.[2] In principle, the accuracy can be improved within the framework of the flat-source collision probability approach by extending the number of regions in the lump. This scheme suffers from the drawback that multiple collision probabilities must be derived, and the numerical work increases substantially. An alternate method is to maintain a single absorber region, but to relax the flat source restriction. This approach is examined cursorily in this note.

The inadequacy of the conventional resonance treatment of highly scattering resonances was demonstrated for the 18.8 eV level of W^{186}. The level parameters are given in Table I, and the Doppler-broadened capture and scattering cross sections at $300^{\circ}K$ are plotted in Fig. 1. The conventional flat-source calculations were performed in slab geometry for several S/M values with the GAROL code.[3] "Exact" calculations incorporating a fine spatial mesh were performed in the S_8 approximation with the GAPLSN DSN transport code.[4] 48 energy groups between 27.85 and 10.38 eV were included. The calculated resonance integrals in this energy range are compared for five values of S/M in Table II. The flat source results are considerably in error at very low values of S/M. The agreement improves with increasing values of S/M. The 2.8% deviation at infinite dilution is a limitation of the GAPLSN 48-group quadrature (3000 mesh points were used in the GAROL calculation). The last column in Table II gives the results of calculations performed on a

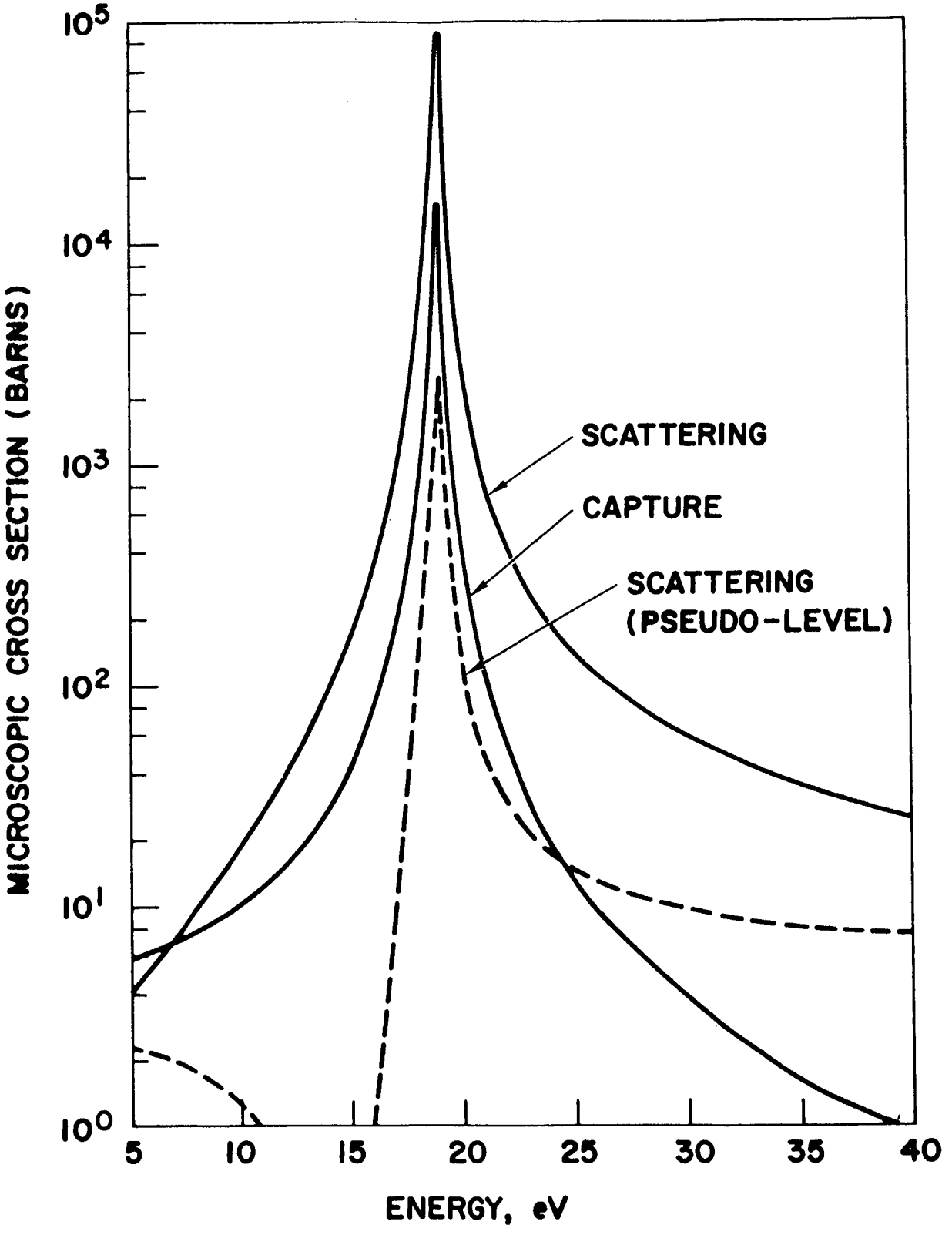

Fig. 1--Scattering and Capture Cross Sections of W^{186}

Table I

Resonance Parameters for 18.8 eV Level of W^{186}

E_o(eV)	Γ_n(mV)	Γ_γ(mV)	Γ_n^o	g
18.83	317	52	72.5	1

Table II

Computed Resonance Integrals of W^{186}
Between 10.38 and 27.85 eV

S/M	Resonance Integral (barns) "Exact" GAPLSN Calculation	Conventional Flat Source Calculation	Percentage Deviation
0.25	24.03	28.60	+ 19.0%
1.00	53.05	60.07	+ 13.0%
6.25	131.18	139.37	+ 6.2%
25.00	238.70	241.52	+ 1.2%
10,000.00 (Infinite dilution)	526.23	511.89	- 2.8%
	With Γ_n and Γ_γ Switched		
0.25	29.22	29.74	+ 1.8%

"pseudo-level", obtained by switching the resonance widths, Γ_n and Γ_γ, in generating the cross sections. This scheme leaves the capture cross section invariant, but diminishes the scattering cross section substantially, as seen in Fig. 1. The close agreement between the conventional and "exact" calculations for the "pseudo-level" indicates that the basis for the prior discrepancy lies in the exceedingly large scattering component of the level.

A physical argument for the shortcoming of the flat source approximation is as follows. If the scattering component of a resonance is small, the exact distribution of the source used to compute the escape probability is unimportant since nearly every neutron entering a lethargy interval is absorbed. The flat source distribution is chosen for convenience as it simplifies the computation of the escape probabilities. However, if the scattering component is large, a description of the source distribution is necessary in order to compute the collision density accurately. This argument can be seen from the integral energy equation, which is given by:

$$F_o(u) = (1 - P_o)\frac{1}{\alpha_o}\int_{u-\Delta_o}^{u} F_o(u')\frac{\sigma_{s_o}}{\sigma_{t_o}}du' + P_1\sigma_{t_1}\frac{e^u}{E_1}, \qquad (1)$$

utilizing the nomenclature of Nordheim.[1] The narrow resonance approximation has been applied in the moderator. If σ_{s_o} is small, the primary contribution to the collision density comes from the second term on the right-hand-side of Eq. (1). In the moderator, the flat source assumption is an adequate approximation, since source neutrons arrive from much lower lethargies where the flux is flat, which is consistent with the narrow resonance approximation. Thus a reasonable estimate for P_1 is obtained by the reciprocity theorem:

$$(P_1)_F = \frac{\sigma_{t_o}}{\sigma_{t_1}}(P_o)_F, \qquad (2)$$

where the subscript, F, denotes flat source. If σ_{s_o} is large, the integral term in Eq. (1) is significant, and the magnitude of P_o is important to the calculation of the collision density. A flat source in the lump is clearly in error because source neutrons at lethargy intervals near the center of the resonance arrive from adjacent, flux-depressed lethargy intervals.

The foregoing discussion suggests that the flat source restriction be retained in the moderator, but that it be relaxed in the lump. The escape probability for the lump is given by:

$$P_o = \frac{\int_{V_o} q_o(\bar{r}) p(\bar{r}) d^3 r}{\int_{V_o} q_o(\bar{r}) d^3 r} , \tag{3}$$

where $q_o(\bar{r})$ is the source distribution and $p(\bar{r})$ is the probability that a neutron born at $\bar{r}$ suffers its first collision outside of the lump. In slab geometry we have:[5]

$$p(z) = \frac{1}{2} \left[E_2(\Sigma_o z) + E_2(\Sigma_o (a - z)) \right] , \tag{4}$$

where a is the thickness of the slab, Σ_o is the total macroscopic cross section, and E_2 is the second order exponential integral. A reasonable and convenient estimate for q_o is given by:*

$$q_o(z) \sim \cosh \left(K_o (z - \frac{a}{2}) \right) , \tag{5}$$

the solution of the source-free, monoenergetic diffusion equation for the flux distribution within the slab, with K_o given by:

$$K_o = \sqrt{3 \Sigma_a \Sigma_o} . \tag{6}$$

Σ_a is the macroscopic absorption cross section of the slab and Σ_o is the total cross section, as before. Using (4) and (5) in Eq. (3), we obtain for the escape probability:

*The origin is taken at one edge of the slab.

$$P_o = \frac{1}{2}\left\{1 + E_2(\Sigma_o a) + \frac{\Sigma_o}{K_o}\coth\left(\frac{K_o a}{2}\right) E_1(\Sigma_o a)\right.$$

$$- \frac{\Sigma_o}{2K_o \sinh\left(\frac{K_o a}{2}\right)}\left[e^{\frac{K_o a}{2}}\left\{\ell n\left(1 + \frac{K_o}{\Sigma_o}\right) + E_1\left(\Sigma_o a\left(1 + \frac{K_o}{\Sigma_o}\right)\right)\right\}\right. \qquad (7)$$

$$\left.\left. + e^{\frac{-K_o a}{2}}\left\{\ell n\left(\left|1 - \frac{K_o}{\Sigma_o}\right|\right) + E_1\left(\Sigma_o a\left(1 - \frac{K_o}{\Sigma_o}\right)\right)\right\}\right]\right\},$$

where E_1 is the first order exponential integral. For small values of $\Sigma_o a$, the escape probability approaches the flat source limit, whereas for large values of $\Sigma_o a$ the escape probability approaches a constant, rather than the flat source limit of zero.

The GAROL code has been modified to accommodate P_o according to Eq. (7) and P_1 from flat source reciprocity, Eq. (2). For slab geometry, the flat source escape probability is given by:

$$(P_o)_F = \frac{1}{\Sigma_o a}\left[\frac{1}{2} - E_3(\Sigma_o a)\right], \qquad (8)$$

where E_3 is the third order exponential integral. The W^{186} resonance integrals, previously obtained by the conventional flat source approximation, were recomputed using the modified escape probabilities, and the results are given in Table III.

The results for the cosh source distribution, given in Table III, are in good agreement with the results of the transport calculations. The prior discrepancy due to the flat source approximation for a large scattering resonance has been eliminated. Furthermore, the agreement for the heavily absorbing "pseudo-level", given in the last row of Table III, has even been slightly improved.

Table III

Computed Resonance Integrals of W^{186} Between 10.38 and 27.85 eV

S/M	"Exact" GAPLSN Calculation	Cosh Source Calculation	Percentage Deviation
	Resonance Integral (barns)		
0.25	24.03	23.94	- 0.4%
1.00	53.05	52.66	- 0.7%
6.25	131.18	130.25	- 0.7%
25.00	238.70	236.20	- 1.0%
10,000.00 (Infinite dilution)	526.23	511.90	- 2.7%
	With Γ_n and Γ_γ Switched		
0.25	29.22	29.46	+ 0.8%

The departure from the flat source restriction is based upon the diffusion theory solution for the flux distribution within the lump. The escape probabilities from the lump are now a function of absorption cross section in addition to the total cross section, but they can be evaluated analytically at each energy point with only a small percentage increase in computer time. This approach appears to hold considerable promise, however additional, more realistic source distributions are worth investigating. Furthermore, this approach should be evaluated for other geometries.

ACKNOWLEDGMENT

Appreciation is extended to G. C. Pomraning for valuable discussions during the course of this work.

REFERENCES

1. L. W. Nordheim, "A New Calculation of Resonance Integrals," Nucl. Sci. Eng., 12, 457 (1962).

2. D. Shook and D. Bogart, "Effective Resonance Integrals of Separated Tungsten Isotopes," Trans. Amer. Nucl. Soc., 8, 284 (1965).

3. C. A. Stevens and C. V. Smith, "GAROL, A Computer Program for Evaluating Resonance Absorption Including Resonance Overlap," GA-6637 (1965).

4. J. H. Alexander, G. W. Hinman, and J. R. Triplett, "GAPLSN, A Modified DSN Program for the Solution of the One-Dimensional Anisotropic Transport Equation," GA-4972 (1964).

5. K. M. Case, F. de Hoffmann, and G. Placzek, "Introduction to the Theory of Neutron Diffusion," Vol. 1, U.S. Government Printing Office, June 1953.

APPENDIX C

CALCULATION OF THE CADMIUM CUTOFF ENERGY

by

J. C. Peak and J. M. Lovallo

CALCULATION OF THE CADMIUM CUTOFF ENERGY

Gold cadmium ratios were measured at the surface of several fuel elements during Phase I of Contract SNPC-27. The results were compared to analysis in Ref. 1. The cadmium cutoff energy, E_c, was assumed to be 0.414 eV in the analysis for convenience; a better value of the cutoff energy has since been determined by direct calculation.

The definition of the cadmium cutoff energy is that the absorption rate for neutrons of all energies in the detector foil, when the cover is present, be equal to the absorption rate in the foil with an ideal cadmium cover present.[2] The ideal cover has an infinite cross section below E_c and a zero cross section above E_c. Thus the definition may be stated as

$$\int_{\text{Foil}} d^3r \int_{E_c}^{\infty} dE\Sigma(E)\varphi(\bar{r}, E) = \int_{\text{Foil}} d^3r \int_{0}^{\infty} dE\Sigma(E)\varphi'(\bar{r}, E) , \qquad (1)$$

where Σ is the absorption cross section in the foil, and $\varphi(\bar{r}, E)$ and $\varphi'(\bar{r}, E)$ denote the flux in the bare and cadmium-covered foils respectively.

The calculation of E_c was done in the following way: the foil and cadmium cover were represented in slab geometry in the GAPLSN[3] code. A slowing down source in a 0.48-cm thick water region outside of the cadmium cover supplied a flux spectrum similar to that of the core. Equation (1) was then evaluated numerically by calculating the neutrons captured in the foil with and without a cadmium cover. The integrals were evaluated to a top energy of 2.38 eV for convenience. At this energy the optical thickness of an 0.022-in. thick cadmium foil is less than 0.01 of an absorption mean free path, and the integrals above 2.38 eV are virtually identical.

REPORT DISTRIBUTION LIST FOR CONTRACT SNPC-27

NASA Lewis Research Center (1)
Space Nuclear Propulsion Office
21000 Brookpark Road
Cleveland, Ohio 44135
Attn: W. D. Stephenson
Contracting Officer

NASA Lewis Research Center (3+Repro)
21000 Brookpark Road
Cleveland, Ohio 44135
Attn: D. Bogart, Program Manager,
MS 49-2

NASA Lewis Research Center (1)
21000 Brookpark Road
Cleveland, Ohio 44135
Attn: Norman T. Musial

NASA Lewis Research Center (2)
21000 Brookpark Road
Cleveland, Ohio 44135
Attn: Library

NASA Lewis Research Center (1)
21000 Brookpark Road
Cleveland, Ohio 44135
Attn: Report Control Office

NASA Lewis Research Center (1)
21000 Brookpark Road
Cleveland, Ohio 44135
Attn: Technical Utilization Office
MS 3-16

National Aeronautics and Space
Administration (2)
Washington, D. C. 20546
Attn: Nuclear Propulsion Office

Manager (2)
Space Nuclear Propulsion Office
U. S. Atomic Energy Commission
Washington, D. C.
Attn: H. B. Finger

Space Nuclear Propulsion Office (1)
U. S. Atomic Energy Commission
Washington, D. C.
Attn: John Morrisey

U. S. Atomic Energy Commission (3)
Technical Reports Library
Washington, D. C.

U. S. Atomic Energy Commission (3)
Division of Tech. Information Extension
P. O. Box 62
Oak Ridge, Tennessee

NASA Lewis Research Center (1)
21000 Brookpark Road
Cleveland, Ohio 44135
Attn: Nuclear Rocket Technical Office
MS 54-1

NASA Lewis Research Center (1)
21000 Brookpark Road
Cleveland, Ohio 44135
Attn: Leroy B. Humble, MS 49-2

NASA Lewis Research Center (1)
21000 Brookpark Road
Cleveland, Ohio 44135
Attn: Samuel Kaufman, MS 49-2

NASA Lewis Research Center (1)
21000 Brookpark Road
Cleveland, Ohio 44135
Attn: Edward Lantz, MS 49-2

NASA Lewis Research Center (1)
21000 Brookpark Road
Cleveland, Ohio 44135
Attn: John Liwosz, MS 54-1

NASA Lewis Research Center (11)
21000 Brookpark Road
Cleveland, Ohio 44135
Attn: Paul Klann, MS 49-2

NASA Lewis Research Center (1)
21000 Brookpark Road
Cleveland, Ohio 44135
Attn: Daniel Fieno, MS 49-2

NASA Lewis Research Center (1)
21000 Brookpark Road
Cleveland, Ohio 44135
Attn: Donald Shook, MS 49-2

NASA Lewis Research Center (1)
21000 Brookpark Road
Cleveland, Ohio 44135
Attn: Wendel Mayo, MS 49-2

NASA Lewis Research Center (1)
21000 Brookpark Road
Cleveland, Ohio 44135
Attn: Office of Reliability and Quality Assurance

NASA Ames Research Center (1)
Moffett Field, California 94035
Attn: Library

NASA Flight Research Center (1)
P. O. Box 273
Edwards, California 93523
Attn: Library

NASA Goddard Space Flight Center (1)
Greenbelt, Maryland 20771
Attn: Library

Jet Propulsion Laboratory (1)
4800 Oak Grove Drive
Pasadena, California 91103
Attn: Library

NASA Langley Research Center (1)
Langley Station
Hampton, Virginia 23365
Attn: Library

NASA Manned Spacecraft Center (1)
Houston, Texas 77001
Attn: Library

NASA Marshall Space Flight Center (1)
Huntsville, Alabama 35812
Attn: Library

NASA Western Operations Office (1)
150 Pico Blvd.
Santa Monica, California 90406
Attn: Library

General Electric Company (1)
Nuclear Materials and Propulsion Operations
P. O. Box 15132
Evendale, Ohio 45215
Attn: R. W. Briskin

Union Carbide Corporation (1)
Nuclear Division
P. O. Box X
Oak Ridge, Tennessee
Attn: R. C. Block

United Nuclear Corporation (1)
Development Division
5 New Street
White Plains, New York
Attn: D. Spielberg

Westinghouse Electric Corporation (1)
Astronuclear Laboratory
P. O. Box 10864
Pittsburgh 36, Pennsylvania

Aerojet General Nucleonics (1)
P. O. Box 77
San Ramon, California 94583
Attn: R. W. Durante

Argonne National Laboratory (1)
P. O. Box 299
Lemont, Illinois
Attn: J. F. Marchaterre
Project Manager, ANL
Nuclear Rocket Study

Brookhaven National Laboratory (1)
Upton, Long Island, New York
Attn: Dr. J. L. Stehn

Combustion Engineering, Inc. (1)
Nuclear Division
500 Prospect Hill Road
Windsor, Connecticut
Attn: Mr. M. Valerino

Los Alamos Scientific Laboratory (3)
Los Alamos, New Mexico
Attn: Dr. R. Spence
N. Division Leader

Atomics International (1)
P. O. Box 309
8900 DeSoto Avenue
Canoga Park, California
Attn: Mr. Martin Berg

NASA Scientific & Technical
Information Facility (6)
Box 5700
Bethesda, Maryland
Attn: NASA Representative

AEC-NASA Space Nuclear Propulsion
Office
Germantown, Maryland SNPO-W
Washington, D. C. 20545
Attn: Milton Klein (1)
F. Carl Schwenk (1)
Paul George Johnson (1)

NASA Lewis Research Center
Space Nuclear Propulsion Office
21000 Brookpark Road
Cleveland, Ohio 44135
Attn: Lester C. Corrington (1)
Richard C. Wilke (1)
Eugene J. Ziurys (1)
Robert W. Schroeder (1)
Morton Fleishman (1)

Argonne National Laboratory
9700 South Cass Avenue
Argonne, Illinois 60440
Attn: B. Spinrad (1)
W. B. Loewenstein (1)
W. Y. Kato (1)
D. Okrent (1)

Atomics International Division
North American Aviation, Inc.
8900 DeSoto Avenue, Box 309
Canoga Park, California 91304
Attn: H. A. Morewitz (1)

Babcock and Wilcox
Lynchburg, Virginia 24504
Attn: H. S. Baninger (1)
T. C. Engelder (1)

Battelle Memorial Institute
505 King Avenue
Columbus, Ohio 43201
Attn: D. A. Dingee (1)

Brookhaven National Laboratory
Upton, Long Island, New York 11101
Attn: J. Chernik (1)
H. Kouts (1)

Combustion Engineering, Inc.
Nuclear Division
500 Prospect Hill Road
Windsor, Connecticut 06095
Attn: J. Dietrich (1)

Donald W. Douglas Research Laboratories
Santa Monica, California 90406
Attn: Ralph S. Cooper (1)

Electro-Optical Systems, Inc.
300 N. Halsted Street
Pasadena, California 91107
Attn: Robert W. Bussard (1)

General Electric Co.
Nuclear Materials and Propulsion Operations
P. O. Box 2147
Idaho Falls, Idaho 83401
Attn: J. W. Morfitt (1)
G. D. Pincock (1)

General Electric Company
Atomic Products Division
175 Curtner Avenue
P. O. Box 254
San Jose, California 95150
Attn: Gerald T. Petersen (1)

Knolls Atomic Power Laboratory
Schenectady, New York 12301
Attn: Richard Ehrlich (1)

Lawrence Radiation Laboratory
P. O. Box 808
Livermore, California 94550
Attn: Theodore Merkel (1)

Lockheed Missiles and Space Company
P. O. Box 504
Sunnyvale, California 94088
Attn: Howard Schmidt (1)

Los Alamos Scientific Laboratory
P. O. Box 1663
Los Alamos, New Mexico 87544
Attn: R. E. Schreiber (1)
Frank Durham (1)
Gordon E. Hansen (1)

Oak Ridge National Laboratory
P. O. Box Y
Oak Ridge, Tennessee 37831
Attn: J. A. Harvey (1)

Rocketdyne Division
North American Aviation Corporation
6633 Canoga Avenue
Canoga Park, California 91304
Attn: Frank Pittman (1)
Jack Armstrong (1)

TRW, Inc.
23555 Euclid Avenue
Cleveland, Ohio 44117
Attn: R. K. Plebuch (1)

U. S. Atomic Energy Commission
Germantown, Maryland
Washington, D. C. 20545
Attn: P. B. Hemmig (1)
G. Rogosa (1)

Westinghouse Electric Corporation
Atomic Power Division
Pittsburgh, Pennsylvania 15230
Attn: Paul Cohen (1)

Catholic University
Washington, D. C. 20017
Attn: R. W. Deutsch (1)